| OF |
AD-
A074379

END
DATE
FILMED
11-79
DDC

NATIONAL BUREAU OF STANDARDS
MICROCOPY RESOLUTION TEST CHART

A074379

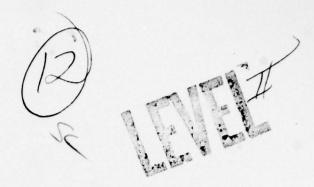# U.S. ARMY MISSILE RESEARCH AND DEVELOPMENT COMMAND

Redstone Arsenal, Alabama 35809

DMI FORM 1000, 1 APR 77

(12)

LEVEL II

TECHNICAL REPORT T-79-41

PERFORMANCE STUDY OF A TWO-DIMENSIONAL CFAR SIGNAL PROCESSOR

Neal B. Lawrence
Advanced Sensors Directorate
Technology Laboratory

and

Jerry D. Moore
Department of Electrical Engineering
University of Alabama
University, Alabama 35486

DDC
RECEIVED
SEP 28 1979
A

26 March 1979

79 09 27 027

18 DRDMI-T

19

REPORT DOCUMENTATION PAGE		READ INSTRUCTIONS BEFORE COMPLETING FORM
1. REPORT NUMBER T-79-41	2. GOVT ACCESSION NO.	3. RECIPIENT'S CATALOG NUMBER
4. TITLE (and Subtitle) 6 Performance Study of a Two-Dimensional CFAR Signal Processor.		5. TYPE OF REPORT & PERIOD COVERED 9 Technical Report. 6. PERFORMING ORG. REPORT NUMBER 14 CSC/TR-77/5487
7. AUTHOR(s) 10 Neal B. Lawrence MIRADCOM and Jerry D. Moore University of Alabama		8. CONTRACT OR GRANT NUMBER(s) 15 DAAH03-75-A-0045 = CSC
9. PERFORMING ORGANIZATION NAME AND ADDRESS US Army Missile Research and Development Command Redstone Arsenal, AL 35809 Dept of Electrical Engineering University of Alabama University, Alabama 35486		10. PROGRAM ELEMENT, PROJECT, TASK AREA & WORK UNIT NUMBERS
11. CONTROLLING OFFICE NAME AND ADDRESS Commander US Army MIRADCOM ATTN: DRDMI-TI Redstone Arsenal, AL 35809		12. REPORT DATE 11 26 March 1979 13. NUMBER OF PAGES 80
14. MONITORING AGENCY NAME & ADDRESS(if different from Controlling Office) 12 81 p.		15. SECURITY CLASS. (of this report) Unclassified 15a. DECLASSIFICATION/DOWNGRADING SCHEDULE

16. DISTRIBUTION STATEMENT (of this Report)

Approved for public release; distribution unlimited.

17. DISTRIBUTION STATEMENT (of the abstract entered in Block 20, if different from Report)

18. SUPPLEMENTARY NOTES

19. KEY WORDS (Continue on reverse side if necessary and identify by block number)

Constant False Alarm Rate	Finite Impulse Response
Two-dimensional CFAR	Moving Target Indicator
Radar	Fixed Window
Digital Signal Processor	Moving Window
	Window Functions

20. ABSTRACT (Continue on reverse side if necessary and identify by block number)

State-of-the-art integrated circuit technology has made it feasible to implement complicated radar signal processors. One candidate for use in radar systems with heavy ground clutter and weather environments is a two-dimensional (2-D) CFAR processor with clutter map. Previous work has established an analytical capability for determining processor performance.

In this report, the dependence of processor performance on moving target indicator structures (i.e., various N-tap finite impulse response filters),

DD FORM 1473 1 JAN 73 EDITION OF 1 NOV 65 IS OBSOLETE

409 723

moving target indicator implementation (i.e., moving window or fixed window methods) and processor window function (i.e., Kaiser, Taylor, Dolph-Chebyshev or rectangular) is discussed.

It is shown that processor performance is almost independent of moving target indicator structure but dependent on moving target indicator implementation. It is also shown that processor performance is dependent on the window function utilized but that finding the "optimum" window function requires knowledge of clutter characteristics.

The significance of this effect has been to establish a means by which processor performance can be determined for various processor configurations and to present results which provide a general understanding of the performance effect of various processor elements.

One important finding was the aliasing problem created by a fixed window moving target indicator when followed by a fast Fourier transform.

ACKNOWLEDGMENT

Huntsville, AL

Accession For		
NTIS GRA&I		☑
DDC TAB		☐
Unannounced		
Justification		
By		
Distribution/		
Availability Codes		
Dist	Avail and/or special	
A		

CONTENTS

1

ILLUSTRATIONS

ILLUSTRATIONS

ILLUSTRATIONS

ILLUSTRATIONS (Concluded)

1. INTRODUCTION

The work documented by this report was initiated by the need and desire to better understand the performance characteristics of radar signal processors. State-of-the-art integrated circuit technology has made it feasible to implement complicated system structures. One candidate for use in radar systems with heavy ground clutter and weather clutter environments is a two-dimensional (2-D) CFAR processor with clutter map. Raytheon Company performed an analysis of this type of a processor under contract with the US Army Missile Command at Redstone Arsenal.[1] The Raytheon effort represents a major contribution to establishing an analytical technique for use with 2-D CFAR signal processors. A detailed study of the Raytheon work was required so that each step of the highly mathematical analysis could be justified. Section 2 presents the results of the review of the theoretical analysis. Section 3, 4 and 5 document the performance results obtained after modification of the computer programs. The main topics studied were the effects that MTI structures, MTI implementations and window functions have on the probability of detection. Section 6 presents a list of proposed extensions to the analysis. The appendices provide further explanation of particular processor occurrences.

2. REVIEW OF THEORETICAL PERFORMANCE ANALYSIS

The block diagram for the processor is shown in <u>Figure 1</u>. This is a linear system up to the point where $\overline{Z}$ is calculated. The input $\overline{\upsilon}$ is represented as a column matrix of the complex (i.e., I and Q channels) input sample values. It follows that

$$\overline{\zeta} = \overline{A}\ \overline{\upsilon} \tag{1}$$

$$\overline{W} = \overline{C}\ \overline{\zeta} \tag{2}$$

$$\overline{F} = \overline{D}\ \overline{W}\ \cdot \tag{3}$$

---

1. Raytheon Company, <u>Automatic Threshold Detector Techniques</u>, Final Report on Contract No. DAAH01-76-C-0363 for US Army Missile Command, ER76-4208, 15 July 1976.
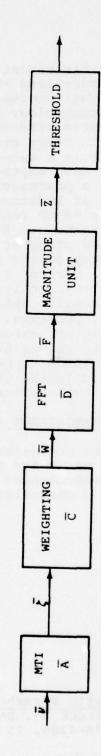
Figure 1. Processor structure.

Due to the linearity, the output at $\bar{F}$ can be described by a Gaussian distribution when Gaussian signals are the input to the system. Also, the input can be separated into a sum of components, viz., ground clutter, weather clutter, noise, and target signal. Each component can be analyzed separately using superposition. The prime objective is to determine the variance at the FFT output. This is a mathematically tractable problem for the Gaussian signals. Let $\bar{M}$ represent the covariance matrix of $\bar{\nu}$, $\bar{M}^{(1)}$ the covariance matrix of $\bar{\zeta}$, and $\bar{M}^{(2)}$ the covariance matrix of $\bar{W}$. It follows that

$$\bar{M}^{(1)} = \bar{A} \; \bar{M} \; \bar{A}^{T} \tag{4}$$

$$\bar{M}^{(2)} = \bar{C} \; \bar{M}^{(1)} \; \bar{C}^{T} . \tag{5}$$

A similar transformation could be used to find the co-variance matrix of $\bar{F}$. However, this is not necessary because the variance of each element of $\bar{F}$ is all that is required. Consequently, the analysis uses the FFT algorithm, superposition of the I and Q signals, and separation of the real and imaginary parts of the F_k element of $\bar{F}$ to obtain

$$\sigma^2_{Rk} = \sum_{i,j=1}^{L} m_{ij} \, c_{ik} \, c_{jk} \tag{6}$$

$$\sigma^2_{Ik} = \sum_{i,j=1}^{L} m_{ij} \, d_{ik} \, d_{jk} \tag{7}$$

where m_{ji} terms are the elements of $\bar{M}^{(2)}$

$$c_{jk} = \cos\left[\frac{2\pi}{L} (j-1) \, k \right] \tag{8}$$

$$d_{jk} = \sin\left[\frac{2\pi}{L} (j-1) \, k \right] \tag{9}$$

9

and the k subscript on the variance represents the kth frequency cell of the FFT output. Combining the I and Q channel results yields the real part of F_k, i.e., $R(F_k)$, and the imaginary part of F_k, i.e., $I(F_k)$, to each be normal with variance $\sigma_{Rk}^2 + \sigma_{Ik}^2$ i.e.,

$$R(F_k) \text{ and } I(F_k) \in N(0, \sigma_{Rk}^2 + \sigma_{Ik}^2). \tag{10}$$

This result holds for the jth range bin and the kth frequency cell for either ground clutter, weather clutter or noise. A change in notation is used to represent this feature, viz., for noise N

$$\sigma_{Njk}^2 = \sigma_{NRk}^2 + \sigma_{NIk}^2. \tag{11}$$

Similar results hold for weather clutter, W, and ground clutter, g. Thus,

$$\sigma_{jk}^2 = \sigma_{Nj_k}^2 + \sigma_{Wj_k}^2 + \sigma_{gj_k}^2. \tag{12}$$

The magnitude unit will change the Gaussian distribution of F_{jk} into an exponential distribution at Z_{jk}, i.e.,

$$p(Z_{jk}) = \frac{1}{2\sigma_{jk}^2} e^{-Z_{jk}/2\sigma_{jk}^2}. \tag{13}$$

Calculation of the probability of false alarm for a fixed threshold V_{Tk} in the kth frequency cell yields

$$PFA = e^{-Y_{bk}} \tag{14}$$

where

$$Y_{bk} = V_{Tk}/2\sigma_{jk}^2. \tag{15}$$

When CFAR or clutter map techniques are used, the threshold is not fixed but is a random variable. It is possible to calculate the expected value (i.e., average value) of the PFA as

$$\overline{PFA} = \int_0^\infty PFA \; p(Y_{bk}) \; dY_{bk} \qquad (16)$$

The density functions for the threshold are dependent on the CFAR technique. A clutter map approach yields

$$\overline{PFA} = \frac{1}{\left(1 + \dfrac{\beta_k K_1}{M}\right)^M} \qquad (17)$$

where M is the number of scans used to accumulate the clutter map threshold, K_1 is a clutter map constant used to specify a false alarm probability, and β_k is a roll-off factor between clutter map cell (i.e., cell o) and the kth cell.

A 2-D CFAR which averages the kth frequency cell of an N-range-bin window will have

$$\overline{PFA} = \frac{1}{\left(1 + \dfrac{\tau_k K_2}{N}\right)^N} \qquad (18)$$

where τ_k relates the range bin of interest to the range bins over which the CFAR window operates, and K_2 is a threshold constant used to specify a false alarm probability. The development for the probability of detection follows a similar procedure, i.e.,

$$\overline{P}_{Dk} = \int_0^\infty P_{Dk} \; p(Y_{bk}) \; dY_{bk} \; . \qquad (19)$$

11

For a Swerling I target the results are

$$P_{Dk} = e^{-Y_{bk}/(1 + \bar{x})} \tag{20}$$

$$\bar{P}_{Dk} = \begin{cases} \dfrac{1}{\left(1 + \dfrac{\beta_k K_1}{M(1 + \bar{x})}\right)^M} & \text{for clutter map} \\[6mm] \dfrac{1}{\left(1 + \dfrac{\tau_k K_2}{N(1 + \bar{x})}\right)^N} & \text{for 2-D CFAR} \end{cases} \tag{21}$$

where $\bar{x}$ is the signal-to-interference ratio for the range bin and frequency cell of interest.

At a given range, the ground clutter backscatter coefficients are assumed to be constant over the CFAR window. However, a Wiebull distribution $p\,(\sigma^0)$ is assumed for the range dependency on these coefficients. Thus,

$$\langle P_{Dk} \rangle = \int_0^\infty \bar{P}_{Dk}\,(\sigma^0)\,p(\sigma^0)\,d\sigma^0 \ . \tag{22}$$

The developments through Equation (22) are a terse parallel of the Raytheon work. The following presents an explanation of how these procedures are implemented in the Raytheon computer program. The program is a hybrid of equation oriented calculations and Monte Carlo simulation. The Wiebull statistics of Equation (22) are evaluated by Monte Carlo procedures. The selection of the clutter map or 2-D CFAR threshold is not determined by Monte Carlo methods. Instead, the average values of the thresholds from each method are determined and the largest average value is used to select the technique. The mathematical description of this is given below.

12

The clutter map threshold is given as

$$A_k = \beta_k \frac{K_1}{2 M \sigma^2_{\infty}} \sum_{m=1}^{M} z_{\infty m} \tag{23}$$

and the average value is

$$\bar{A}_k = \frac{\beta_k K_1}{2} = \frac{\alpha_k \sigma^2_{\infty}}{2 \sigma^2_{0k}} K_1 \tag{24}$$

where σ^2_{∞} is the variance in the bin of interest and frequency cell 0. The range bins below the bin of interest yield a 2-D CFAR threshold of

$$B_k = \tau_k \frac{K_2}{2N\sigma^2_{-1k}} \sum_{j=-1}^{-N} z_{jk} \tag{25}$$

where σ^2_{-1k} represents the "below" (-1) bins and the kth frequency cell. The average value is

$$\bar{B}_k = \frac{\tau_k K_2}{2} = \frac{K_2}{2} \frac{\sigma^2_{-1k}}{\sigma^2_{0k}} . \tag{26}$$

Similar results hold for the 2-D CFAR threshold determined from the range bins above the bin of interest, i.e., C_k and $\bar{C}_k$.

The program determines

$$\bar{Y}_{bk} = \text{Max} \; (\bar{A}_k, \; \bar{B}_k, \; \bar{C}_k) . \tag{27}$$

The selection process is actually accomplished as

$$2\sigma^2_{0k} \; \bar{Y}_{bk} = \text{Max} \; (\alpha_k K_1 \; \sigma^2_{\infty}, \; K_2 \; \sigma^2_{-1k}, \; K_2 \; \sigma^2_{1k}) \tag{28}$$

13

Once the threshold is selected, then the results of Equation (21) are used to calculate the probability of detection.

An actual radar system with clutter-map and 2-D CFAR would not use the average values as in Equation (27), but would use the maximum of the thresholds A_k, B_k or C_k.

The threshold selection method used by Raytheon saves simulation time on the computer, but appears to be dependent on an intuitive justification. There appears to be a need to improve this part of the analysis and suggestions are offered in Section 6.

3.   PERFORMANCE DEPENDENCE ON MTI STRUCTURE

A 3-pulse canceler and a narrow-notch MTI were used in the analyses performed by Raytheon. It was desirable to investigate the performance of other MTI designs; specifically, a 2-pulse canceler, a 5- and a 9-coefficient Chebyshev design determined by the Houts and Burlage procedure[2,3] and a 26-coefficient bimodal filter designed by Holt[4] to reject ground and weather clutter. It was necessary to modify the computer program to incorporate this capability. The threshold selection technique was also refined to include a parameter that had been omitted in the original program. Subsequently, a number of verification runs were made and the only differences between these and the original results were for the lower numbered frequency cells. These results did not change the relative performance results or the conclusions presented by Raytheon.

2.   R.C. Houts and D.W. Burlage, "Maximizing the Usable Bandwidth of MTI Signal Processors," Institute of Electrical and Electronics Engineers (IEEE) Transactions, on Aerospace and Electronic Systems, Vol. AES-13, No. 1, January 1977, pp. 48-55.

3.   D.W. Burlage and R.C. Houts, Design Techniques for Improved Bandwidth Moving Target Indicator Processors in Surface Radars, US Army Missile Command, Redstone Arsenal, Alabama, Technical Report RE-75-35, 1975.

4.   B.P. Holt, and R.C. Houts, "Multiband FIR Digital Filter Design Algorithm for Radar Clutter Suppression," Record of 1978 IEEE Int. Conf. on Acoustics, Speech and Signal Processing, April 1978.

New results obtained for the 2-, 3-, 5-, and 9-coefficient filters and a ground clutter environment revealed practically the same performance for all systems as shown in Figures 2 through 5. This equivalence of performance can be predicted since all of the MTI filters were approximately equal at rejecting the ground clutter. It might erroneously be expected that the performance of a CFAR system with FFT processing would be totally independent of the MTI. Such faulty reasoning would argue that a given frequency cell would maintain the same signal-to-interference ratio with or without an MTI. However, the finite sample length of the input data train causes sidelobe coupling into other frequency cells. The use of window functions can serve to reduce this effect, but for large ground clutter components there will still be substantial sidelobe levels. The MTI serves to reduce the mainlobe levels and consequently the sidelobes produced by windowing the MTI outputs.

A comparison of the 3-pulse MTI to no MTI is given in Figures 6, 7 and 8 as the spectral width of the ground clutter is changed. These results agree with intuition since for a narrow ground clutter spectrum more of the sidelobe power appear at nulls of the window function.

When weather clutter is added to the input of the 2-, 3-, 5-, and 9-coefficient MTI filters, the performance is degraded as shown in Figures 9 through 12 for various weather conditions. The relative response of the MTI filter over the bandwidth of the weather has a major effect on the sidelobe contributions and thereby on the performance of other frequency cells. It is interesting to note the relative improvements in the performance curves at frequencies between the ground clutter and weather clutter.

The use of the 26-coefficient bimodal filter is effective in rejecting the weather, provided the design parameters are matched to the center frequency and spectral width of the clutter. A satisfactory design is illustrated in Figure 13 where ideal performance is compared to predicted CFAR performance. Comparisons of the bimodal MTI and 3-pulse MTI are given in Figures 14, 15 and 16 for various weather conditions. The improved performance at frequencies between the ground and weather clutters is a result of reducing the sidelobe contributions in these cells. This analysis was performed for a 64-point FFT and this requires 86 input pulses as compared to 66 pulses when the 3-pulse MTI is used. When a 32-point FFT is used with the bimodal MTI, then only 57 pulses are required. A

15

S/N = 10 dB, S/C = -35 dB, 18-Hz GROUND CLUTTER, 40-dB TAYLOR WEIGHTS, 16 RANGE BINS IN CFAR WINDOW, 64-POINT FFT, NO WEATHER

IDEAL

PREDICTED

PROBABILITY OF DETECTION -- %

FREQUENCY CELLS
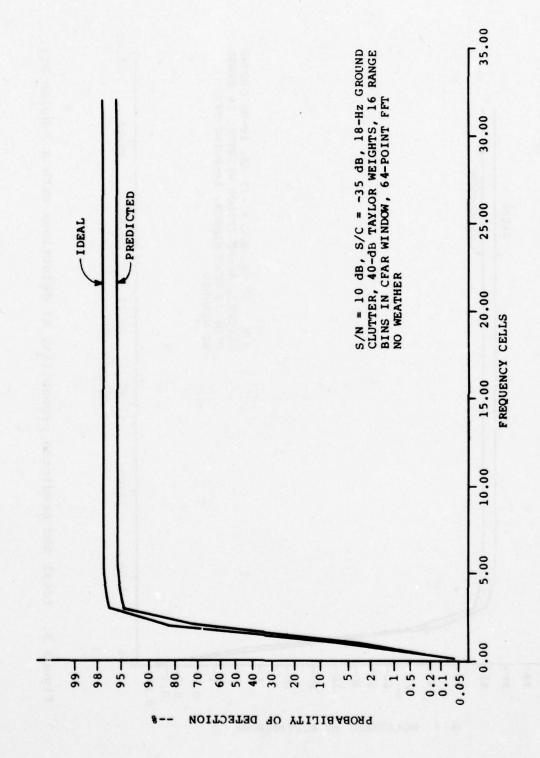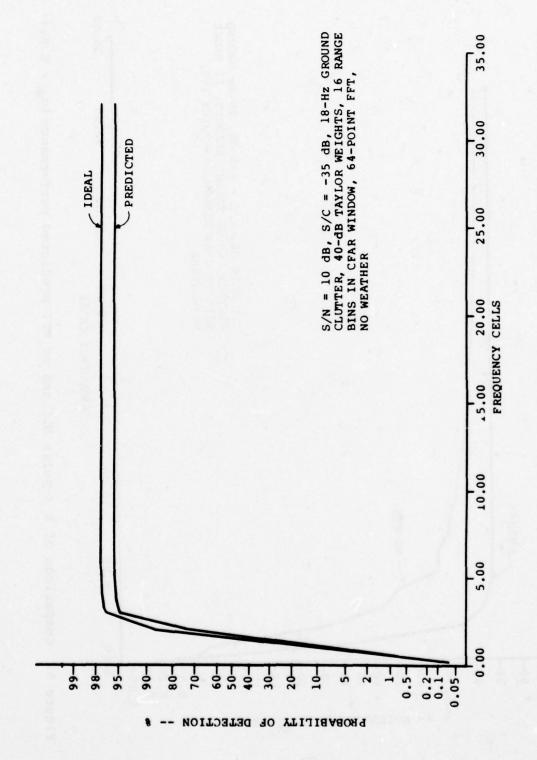
Figure 2. Ideal and predicted probability of detections with a 2-Pulse MTI.

S/N = 10 dB, S/C = -35 dB, 18-Hz GROUND
CLUTTER, 40-dB TAYLOR WEIGHTS, 16 RANGE
BINS IN CFAR WINDOW, 64-POINT FFT,
NO WEATHER
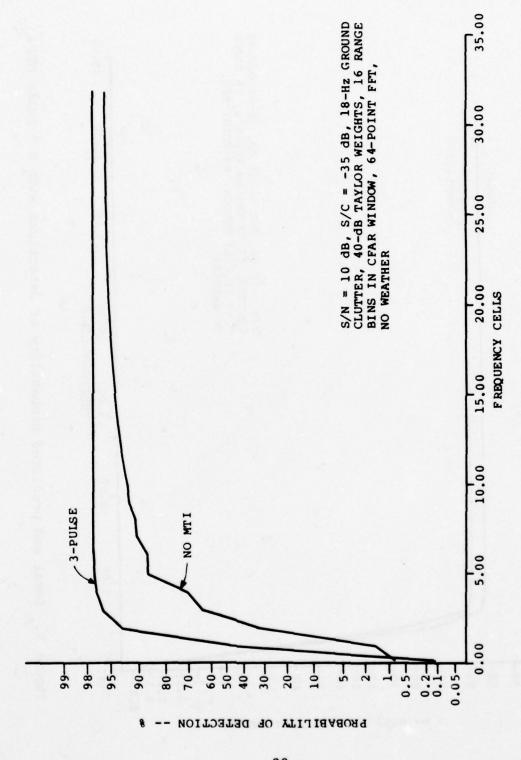
Figure 3. Ideal and predicted probability of detections with a 3-pulse MTI.

17

S/N = 10 dB, S/C = -35 dB, 18-Hz GROUND
CLUTTER, 40-dB TAYLOR WEIGHTS, 16 RANGE
BINS IN CFAR WINDOW, 64-POINT FFT
NO WEATHER

Figure 4. Ideal and predicted probability of detections with a 5-pulse MTI.

18

S/N = 10 dB, S/C = -35 dB, 18-Hz GROUND CLUTTER, 40-dB TAYLOR WEIGHTS, 16 RANGE BINS IN CFAR WINDOW, 64-POINT FFT, NO WEATHER

Figure 5. Ideal and predicted probability of detections with a 9-pulse MTI.

19

S/N = 10 dB, S/C = -35 dB, 18-Hz GROUND CLUTTER, 40-dB TAYLOR WEIGHTS, 16 RANGE BINS IN CFAR WINDOW, 64-POINT FFT, NO WEATHER

Figure 6. Comparison of a 3-pulse MTI and no MTI predicted performance (σ_g = 5 Hz).

20

S/N = 10 dB, S/C = -35 dB, 10-Hz GROUND
CLUTTER, 40-dB TAYLOR WEIGHTS, 16 RANGE
BINS IN CFAR WINDOW, 64-POINT FFT,
NO WEATHER
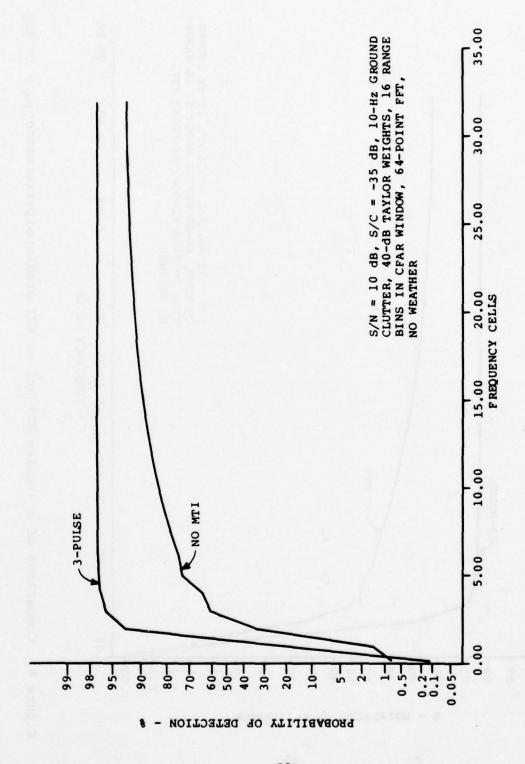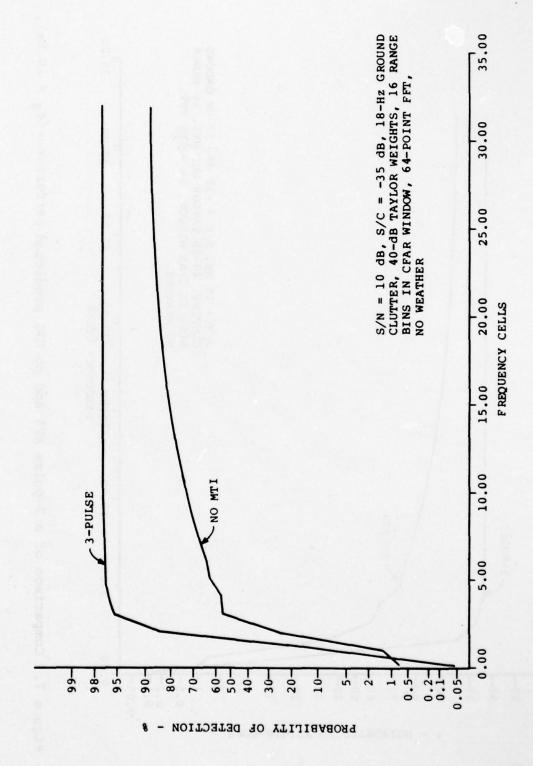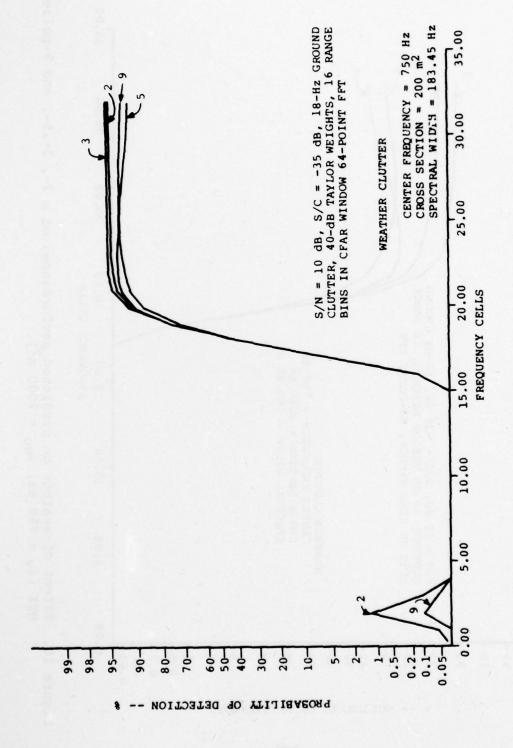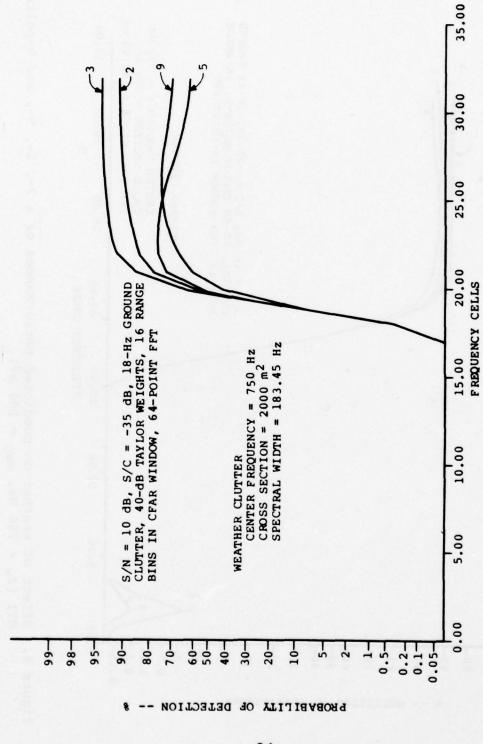
Figure 7. Comparison of a 3-pulse MTI and no MTI predicted performance (q_g = 10 Hz).
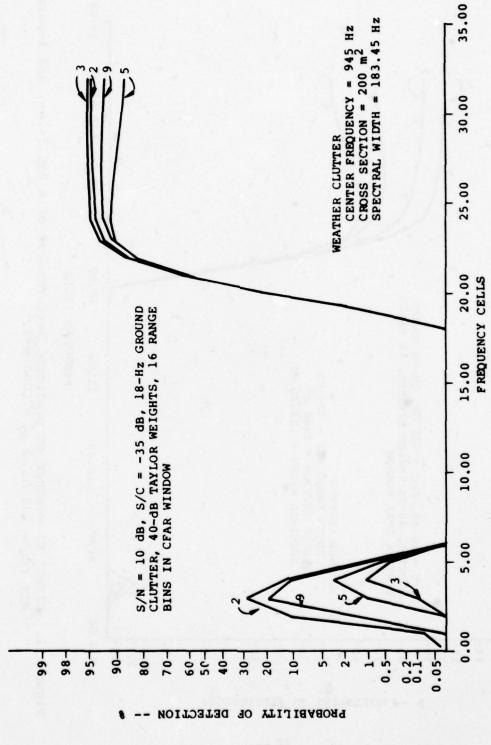
21

S/N = 10 dB, S/C = -35 dB, 18-Hz GROUND
CLUTTER, 40-dB TAYLOR WEIGHTS, 16 RANGE
BINS IN CFAR WINDOW, 64-POINT FFT,
NO WEATHER

Figure 8. Comparison of a 3-pulse MTI and no MTI predicted performance(σ_g = 18 Hz).

22
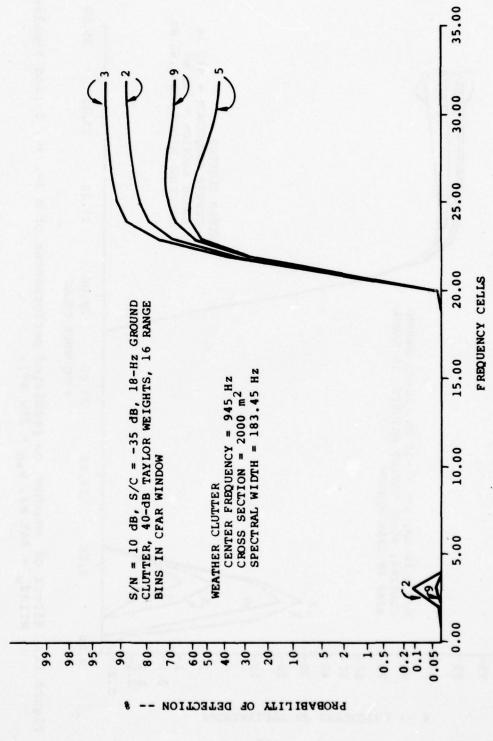
Figure 9. Effect of weather on predicted performances of a 2-, 3-, 5-, and 9-pulse MTI (f_w = 750 Hz, μ_{wo} = 200 m²).

23
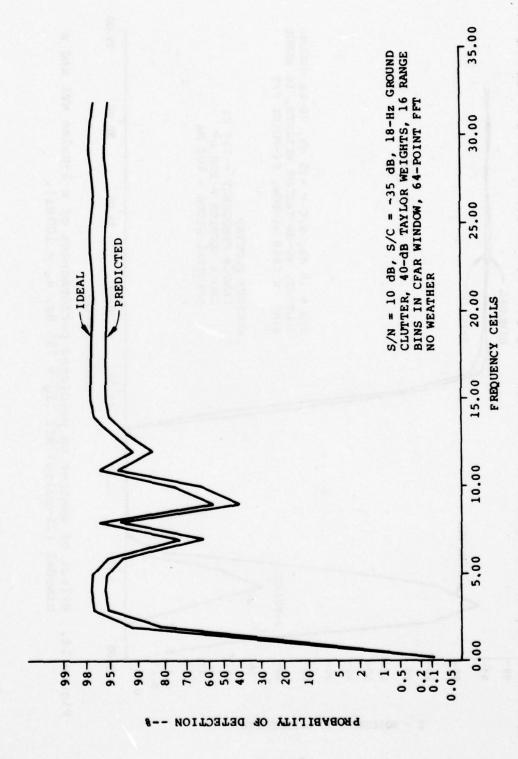
Figure 10. Effect of weather on predicted performances of a 2-, 3-,5-, and 9-pulse MTI (f_w = 750 Hz, μ_{wo} = 2000 m²).

24
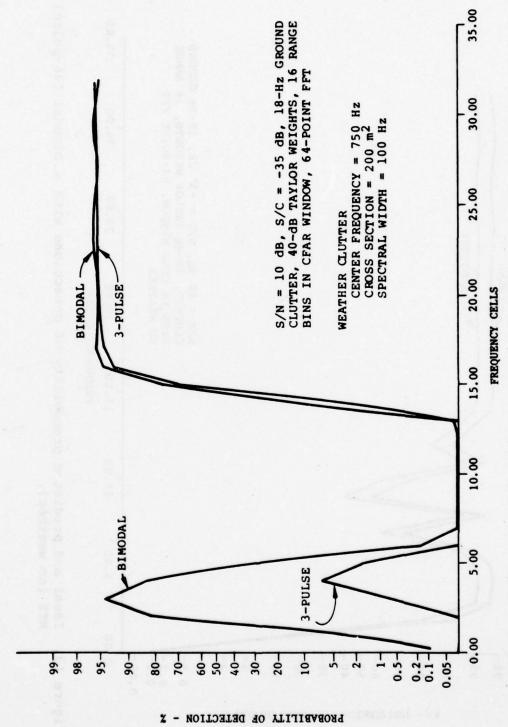
Figure 11. Effect of weather on predicted performances of a 2-, 3-, 5-, and 9-pulse MTI (f_w = 945 Hz, μ_{wo} = 200 m²).

25

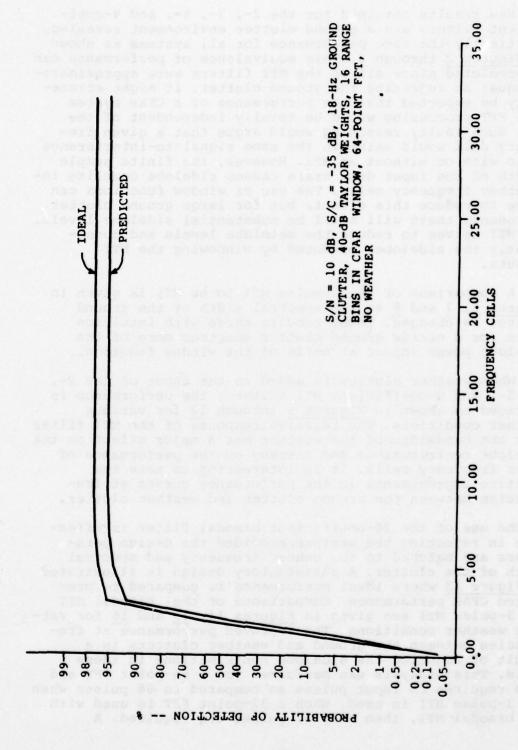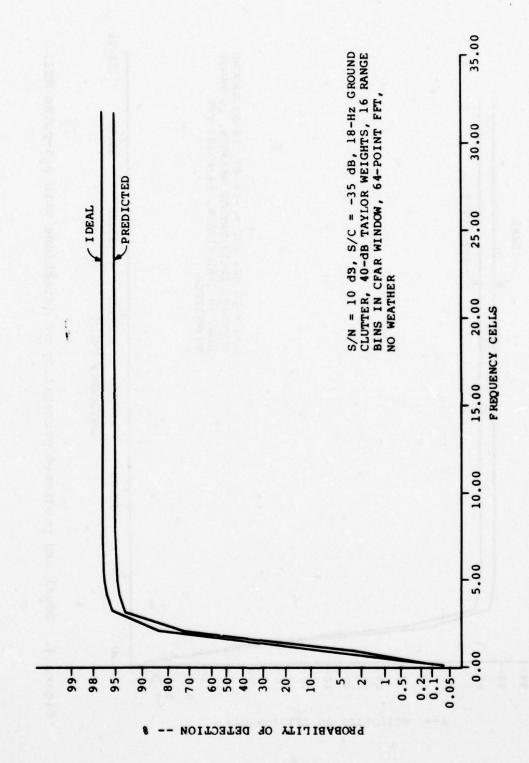Figure 12. Effect of weather on predicted performances of a 2-, 3-, 5-, and 9-pulse MTI (f_w = 945 Hz, μ_{wo} = 2000 m²).

26
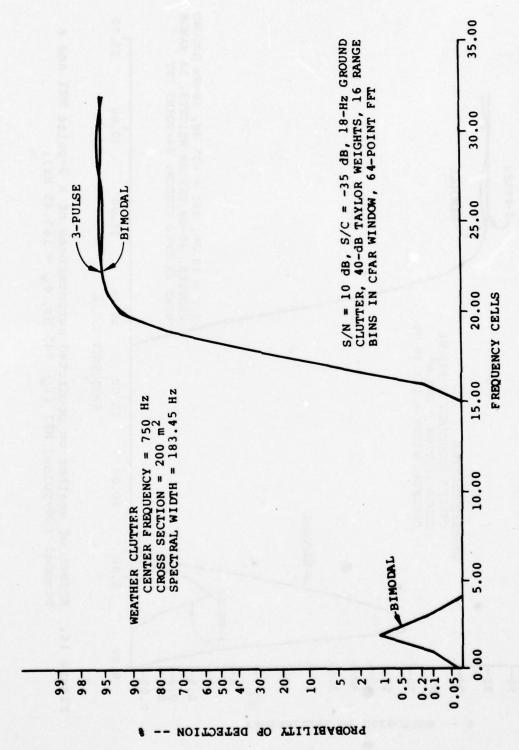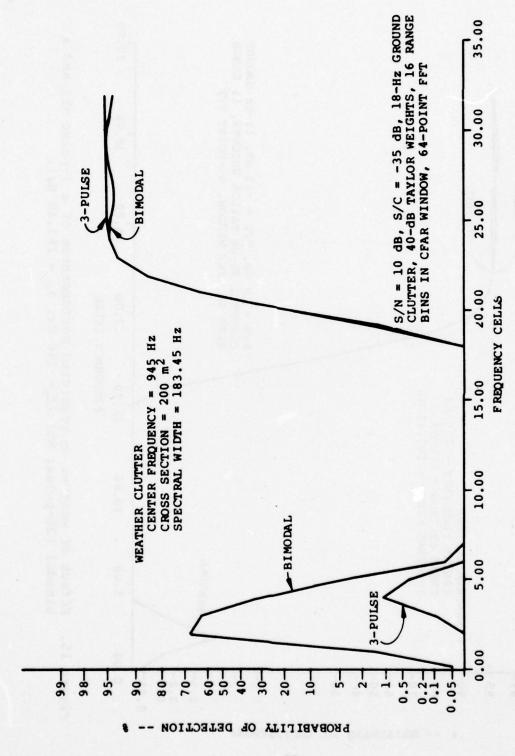
Figure 13. Ideal and predicted probability of detections with a bimodal (26-pulse) MTI (no weather).

S/N = 10 dB, S/C = -35 dB, 18-Hz GROUND
CLUTTER, 40-dB TAYLOR WEIGHTS, 16 RANGE
BINS IN CFAR WINDOW, 64-POINT FFT
NO WEATHER

27

Figure 14. Effect of weather on predicted performances of a 3-pulse MTI and a bimodal (26-pulse) MTI ($\bar{f}_w = 750$ Hz, $\sigma_w = 100$ Hz).

S/N = 10 dB, S/C = -35 dB, 18-Hz GROUND CLUTTER, 40-dB TAYLOR WEIGHTS, 16 RANGE BINS IN CFAR WINDOW, 64-POINT FFT

WEATHER CLUTTER
CENTER FREQUENCY = 750 Hz
CROSS SECTION = 200 m²
SPECTRAL WIDTH = 100 Hz

28

WEATHER CLUTTER
CENTER FREQUENCY = 750 Hz
CROSS SECTION = 200 m^2
SPECTRAL WIDTH = 183.45 Hz

3-PULSE

BIMODAL

S/N = 10 dB, S/C = -35 dB, 18-Hz GROUND
CLUTTER, 40-dB TAYLOR WEIGHTS, 16 RANGE
BINS IN CFAR WINDOW, 64-POINT FFT

BIMODAL

FREQUENCY CELLS

PROBABILITY OF DETECTION -- %

99
98
95
90
80
70
60
50
40
30
20
10
5
2
1
0.5
0.2
0.1
0.05

0.00   5.00   10.00   15.00   20.00   25.00   30.00   35.00

Figure 15. Effect of weather on predicted performances of a 3-pulse MTI and a bimodal (26-pulse) MTI (f_w= 750 Hz, σ_w = 183.45 Hz).

29

WEATHER CLUTTER
CENTER FREQUENCY = 945 Hz
CROSS SECTION = 200 m²
SPECTRAL WIDTH = 183.45 Hz

S/N = 10 dB, S/C = -35 dB, 18-Hz GROUND
CLUTTER, 40-dB TAYLOR WEIGHTS, 16 RANGE
BINS IN CFAR WINDOW, 64-POINT FFT

Figure 16. Effect of weather on predicted performances of a 3-pulse MTI and a bimodal (26-pulse) MTI (f_w= 945 Hz, σ_w = 183.45 Hz).

30

comparison is given in Figures 17 and 18 for the 3-pulse, 64-point FFT and the bimodal, 32-point FFT with and without weather.

The relative performance of the 3-pulse and bimodal MTI structures does not depend on the SNR. This is shown in Figures 19 and 20 for SNRs of 0 dB and 10 dB.

4. PERFORMANCE DEPENDENCE ON MTI IMPLEMENTATION

The MTI used in radar signal processors can be implemented by either an Infinite Impulse Response (IIR) or Finite Impulse Response (FIR) filter. Due to transient and hardware considerations, the finite impulse response is the configuration more often used. There are two major alternatives for realizing the finite impulse response filter. In radar terminology, these have become known by names such as the moving window and the fixed window methods. The implementation methods allow a trade-off between amount of hardware required and signal-to-noise obtained[5]. Raytheon's orginal simulation was based on moving window MTI and, thus, was modified to provide the capability of analysis using the fixed window MTI.

In any radar system, the number of pulses that can be effectively used is limited by several factors, i.e., scan time, range walk, target acceleration and maximum time of target coherence. Therefore, meaningful performance results require maintaining approximately the same number of pulses for different processor configurations. It has been determined that the moving window filter produces K_{MW} residues
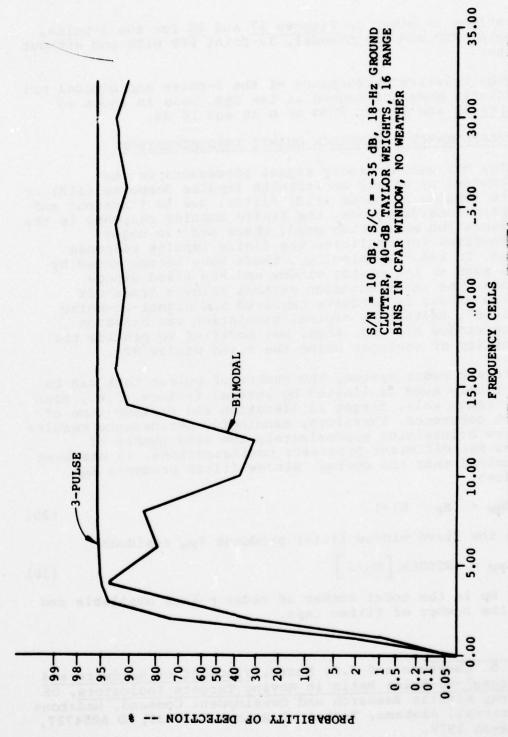
$$K_{MW} = (N_P - N)+1 \qquad (29)$$

while the fixed window filter produces K_{FW} residues
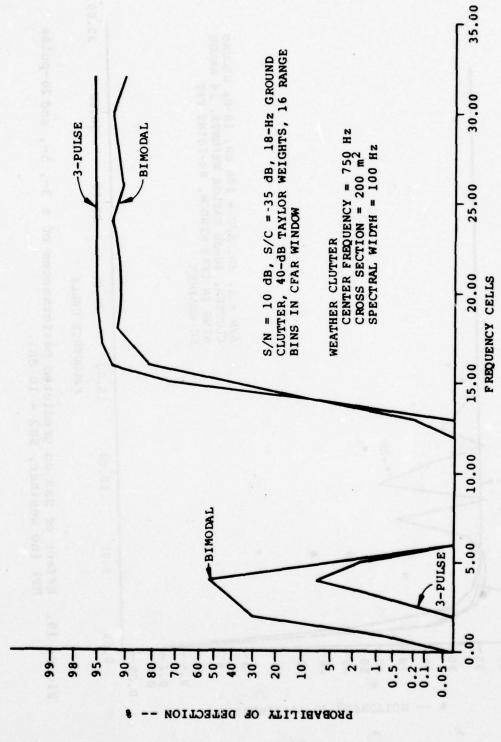
$$K_{FW} = \text{INTEGER} \left[N_P/N \right] \qquad (30)$$

where Np is the total number of radar pulses available and N is the number of filter taps.
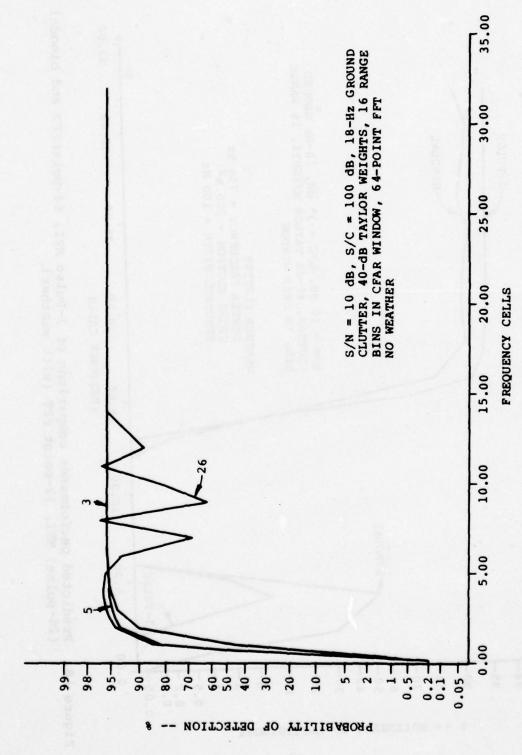
5. N.B. Lawrence and J.D. Moore, Tradeoff of Hardware and Signal-to-Noise Ratio in Moving Targets Indicators, US Army Missile Research and Development Command, Redstone Arsenal, Alabama, Technical Report T-78-39, AD A054727, March 1978.
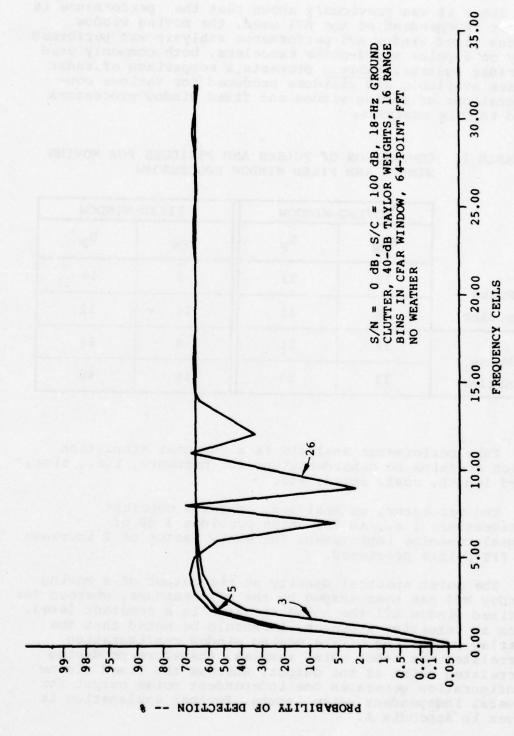
Figure 17. Predicted performance comparison of 3-pulse MTI, 64-point FFT and bimodal (26-pulse) MTI, 32-point FFT (no weather).

32

The graph axes and labels:

PROBABILITY OF DETECTION -- %

FREQUENCY CELLS

S/N = 10 dB, S/C = -35 dB, 18-Hz GROUND
CLUTTER, 40-dB TAYLOR WEIGHTS, 16 RANGE
BINS IN CFAR WINDOW

WEATHER CLUTTER
  CENTER FREQUENCY = 750 Hz
  CROSS SECTION = 200 m²
  SPECTRAL WIDTH = 100 Hz

3-PULSE

BIMODAL

Figure 18. Predicted performance comparison of 3-Pulse MTI, 64-point FFT and bimodal (26-pulse) MTI, 32-point FFT (with weather).

33

S/N = 10 dB, S/C = 100 dB, 18-Hz GROUND CLUTTER, 40-dB TAYLOR WEIGHTS, 16 RANGE BINS IN CFAR WINDOW, 64-POINT FFT NO WEATHER

FREQUENCY CELLS

PROBABILITY OF DETECTION -- %

Figure 19. Effect of SNR on predicted performances of a 3-, 5-, and 26-pulse MTI (no weather, SNR = 10 dB).

Figure 20. Effect of SNR on predicted performances of a 3-, 5-, and 26-pulse MTI (no weather, SNR = 0 dB).

S/N = 0 dB, S/C = 100 dB, 18-Hz GROUND CLUTTER, 40-dB TAYLOR WEIGHTS, 16 RANGE BINS IN CFAR WINDOW, 64-POINT FFT NO WEATHER

PROBABILITY OF DETECTION -- %

FREQUENCY CELLS

Since it was previously shown that the performance is almost independent of the MTI used, the moving window versus fixed window MTI performance analysis was performed only on 2-pulse and 3-pulse cancelers, both commonly used in radar systems. Table 1 presents a comparison of radar pulses available and residues produced for various configurations of moving window and fixed window processors used in this analysis.

TABLE 1. COMPARISON OF PULSES AND RESIDUES FOR MOVING WINDOW AND FIXED WINDOW PROCESSORS

	MOVING-WINDOW		FIXED-WINDOW	
	K_{MW}	N_P	K_{FW}	N_P
2-Pulse Canceler	32	33	8	16
	32	33	16	32
3-Pulse Canceler	32	34	8	24
	32	34	16	48

This performance analysis is a computer simulation which contains no considerations for hardware, i.e., size, word length, cost, speed, etc.

The processor, as analyzed, contains coherent integration, i.e., an FFT which provides 3 dB of signal-to-noise improvement for every factor of 2 increase in FFT points processed.

The noise spectral density at the output of a moving window MTI has been shaped by the MTI response, whereas for a fixed window MTI the noise spectrum is a constant level. From an intuitive approach, it should be noted that the overlap processing of the moving window configuration correlates the input noise samples, therefore, producing correlated noise at the output, whereas the fixed window configuration generates one independent noise output for several independent noise inputs. Further explanation is given in Appendix A.

36
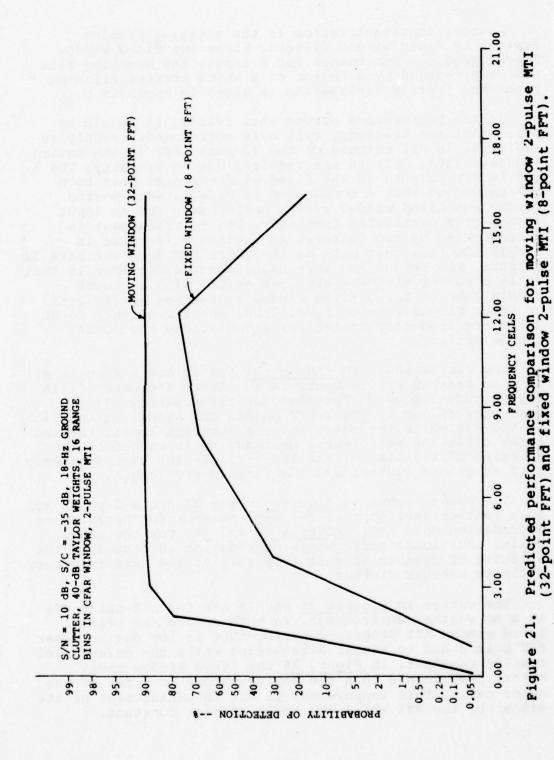
Another important factor is the aliasing problem created by fixed window filters. Since the fixed window filter produces one output for N inputs the sampling rate has been reduced by a factor of N which creates aliasing problems. Further explanation is given in Appendix B.
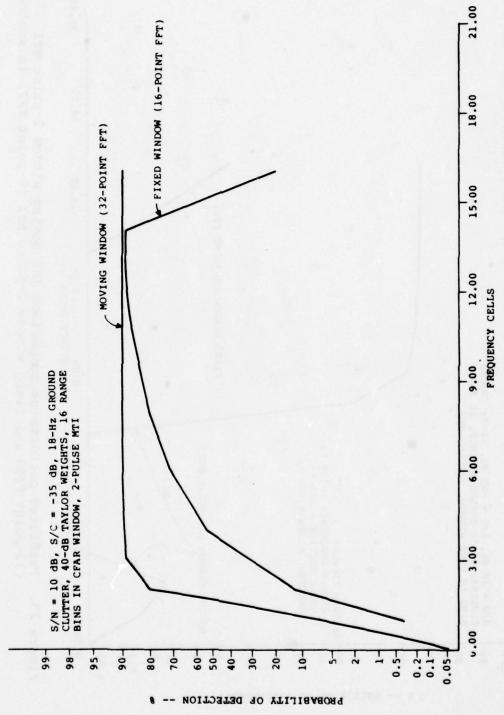
In the performance curves that follow, it should be noted that the frequency cell axis corresponds exactly to the first 16 FFT outputs of the 32-point FFT in the moving window system. Only 16 are required due to symmetry. The 8 and 16 FFT outputs in the fixed window system have been rearranged so that a comparison is made between moving window and fixed window system performance for an input signal of a particular frequency. The rearrangement is necessitated by two factors. An obvious difference is simply the fact that an 8- or 16- point FFT does not have 32 outputs. The second and more significant difference is that while a moving window system has an FFT with an input sample rate of f_s; a fixed window system has an FFT with an input sample rate of f_s/N. Thus, the FFT outputs cover different frequency ranges for fixed window and moving window systems.

The curves shown in Figures 21 and 22 are a 2-pulse MTI in a no weather environment. In the lower frequency cells the degradation in performance for fixed window MTI processor is due to fewer FFT points and signal attenuation by the MTI while the noise is at a constant level. For the upper cells, the performance degradation is caused by the aliasing of signals so that they fall in the same frequency cell as ground clutter and the reduced FFT length.
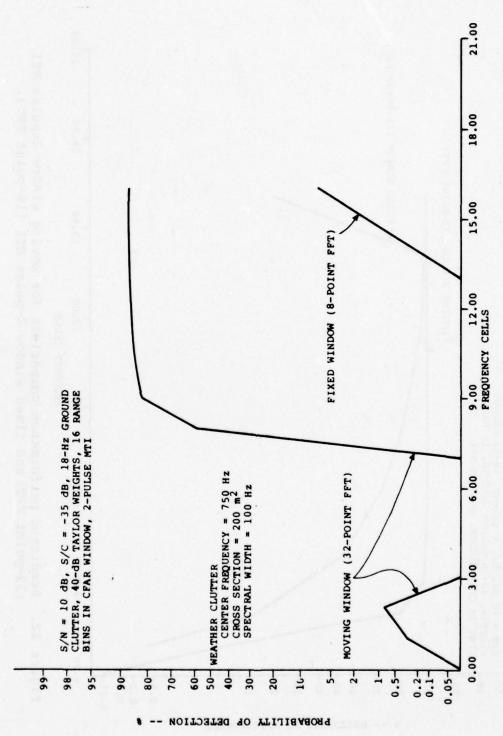
The curves shown in Figures 23 and 24 are a 2-pulse MTI in a weather environment. The same reasons for performance degradation hold as in Figures 21 and 22. For the upper cells, additional performance degradation is caused by the aliasing of signals so that they fall in the same frequency cells as weather clutter.

The curves in Figures 25 and 26 are for a 3-pulse MTI in a no weather environment. In both curves the overall fixed window MTI processor performance is low due to fewer FFT points and to signal attenuation while the noise level remains constant. In Figure 26 the fixed window shows better performance than the moving window in a few of the upper cells. This improvement is due to enhancement of the signal by the MTI while the noise remains constant.
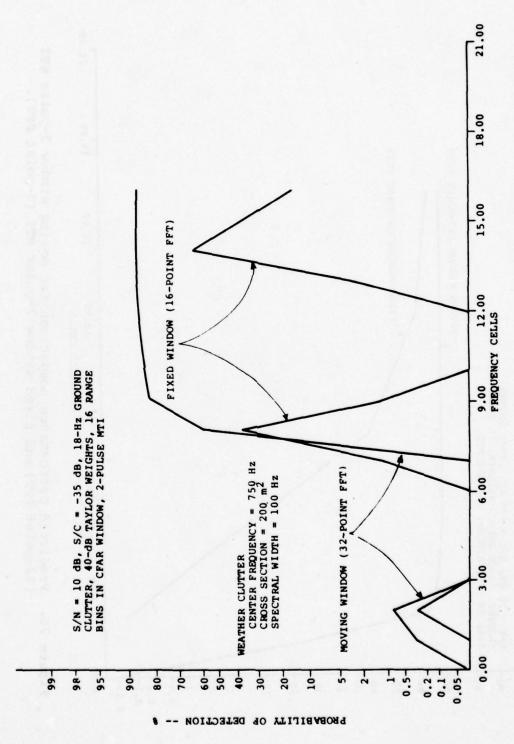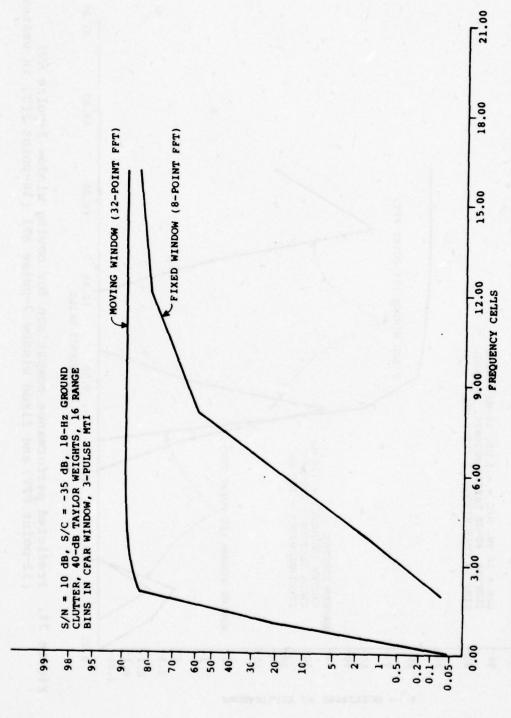
37

Figure 21. Predicted performance comparison for moving window 2-pulse MTI (32-point FFT) and fixed window 2-pulse MTI (8-point FFT).

38

Figure 22. Predicted performance comparison for moving window 2-pulse MTI (32-point FFT) and fixed window 2-pulse MTI (16-point FFT).

39
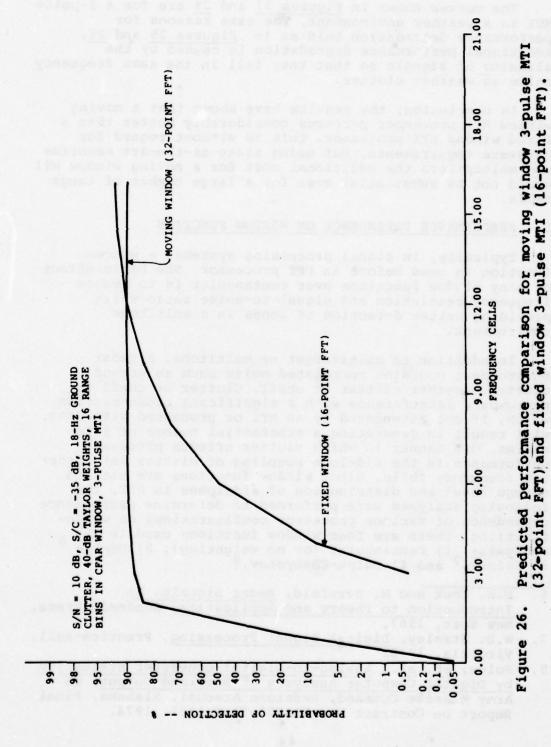
Figure 23. Predicted performance comparison for moving window 2-pulse MTI (32-point FFT) and fixed window 2-pulse MTI (8-point FFT) in weather.

40

Figure 24. Predicted performance comparison for moving window 2-pulse MTI (32-point FFT) and fixed window 2-pulse MTI (16-point FFT) in weather.

S/N = 10 dB, S/C = -35 dB, 18-Hz GROUND
CLUTTER, 40-dB TAYLOR WEIGHTS, 16 RANGE
BINS IN CFAR WINDOW, 3-PULSE MTI

MOVING WINDOW (32-POINT FFT)

FIXED WINDOW (8-POINT FFT)

FREQUENCY CELLS

0.00   3.00   6.00   9.00   12.00   15.00   18.00   21.00

99
98
95
90
80
70
60
50
40
30
20
10
5
2
1
0.5
0.2
0.1
0.05

Figure 25. Predicted performance comparison for moving window 3-pulse MTI
(32-point FFT) and fixed window 3-pulse MTI (8-point FFT).

42

The curves shown in Figures 27 and 28 are for a 3-pulse MTI in a weather environment. The same reasons for performance degradation hold as in Figures 25 and 26. Additional performance degradation is caused by the aliasing of signals so that they fall in the same frequency cells as weather clutter.

In conclusion, the results have shown that a moving window MTI processor performs considerably better than a fixed window MTI processor. This is without regard for hardware requirements. But using state-of-the-art memories and multipliers the additional cost for a moving window MTI would not be substantial even for a large number of range cells.

5. PERFORMANCE DEPENDENCE ON WINDOW FUNCTION
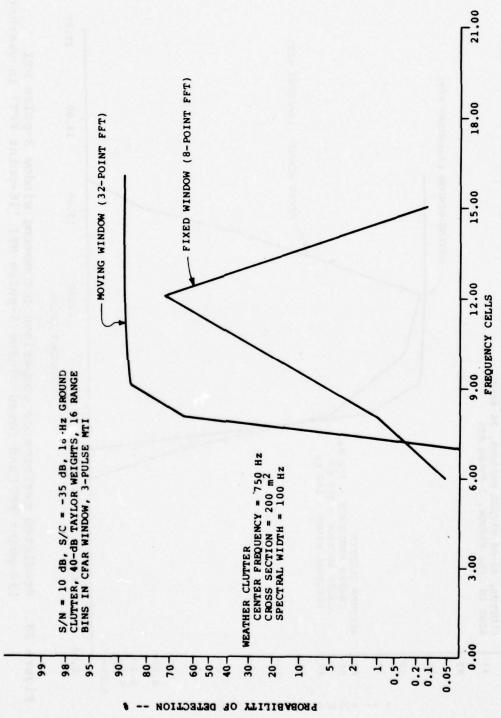
Typically, in signal processing systems, a window function is used before an FFT processor. The basic effect of many window functions over rectangular is to reduce frequency resolution and signal-to-noise ratio while providing better detection of tones in a multitone environment.

In addition to multitarget or multitone, a radar environment contains correlated noise such as ground clutter, weather clutter or chaff. Clutter or chaff is narrowband interference with a significant cross-section which, if not attenuated by an MTI or processed with CFAR, will result in generating a substantial number of false alarms. One manner in which clutter effects processor performance is the sidelobe coupling of clutter into other FFT frequency cells. Since window functions are used to change level and distribution of sidelobes in FFT, the following analyses were performed to determine performance dependence of various processor configurations on window functions. There are four window functions used in the analysis: 1) rectangular (or no weighting), 2) Taylor,[6] 3) Kaiser,[7] and 4) Dolph-Chebyshev.[8]
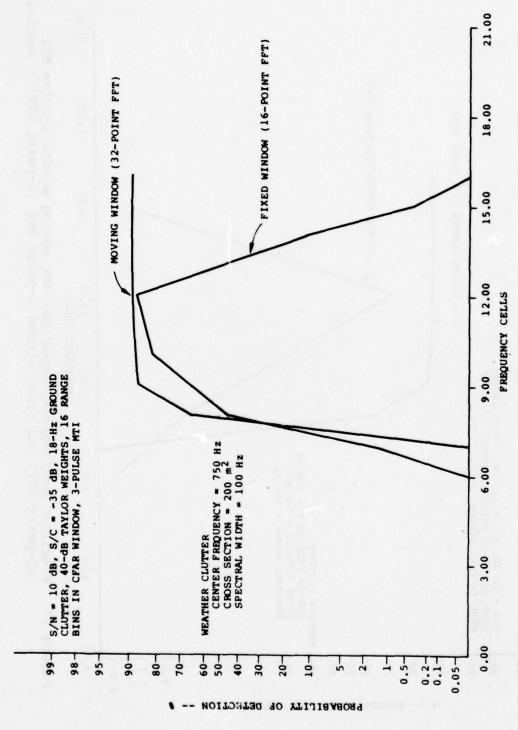
6. E.E. Cook and M. Bernfeld, Radar Signals: An Introduction to Theory and Application, Academic Press, New York, 1967.

7. W.D. Stanley, Digital Signal Processing, Prentice-Hall, Virginia, 1975.

8. Polge, et, al., Analog-to-Digital Converter Evaluation by Digital Computer Analysis of Recorded Output, US Army Missile Command, Redstone Arsenal, Alabama, Final Report on Contract No. DAAH01-71-C-1181, 1974.

Figure 27. Predicted performance comparison for moving window 3-pulse MTI (32-point FFT) and fixed window 3-pulse MTI (8-point FFT), in weather.

45

Figure 28. Predicted performance comparison for moving window 3-pulse MTI (32-point FFT) and fixed window 3-pulse MTI (16-point FFT) in weather.

46
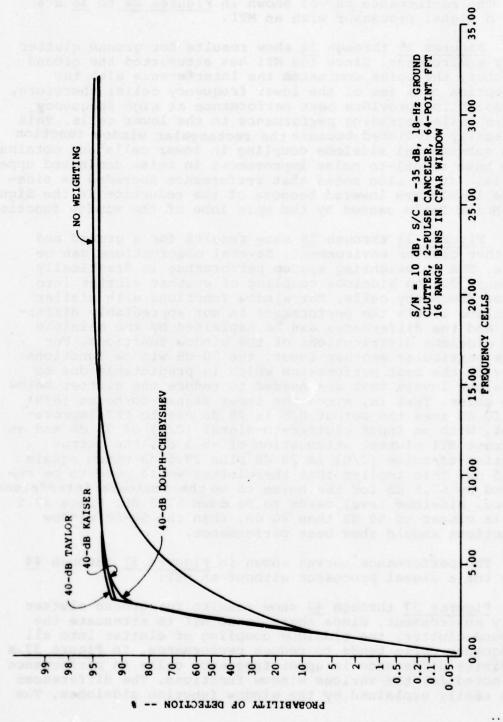
The performance curves shown in Figures 29 to 36 are for a signal processor with an MTI.

Figures 29 through 32 show results for ground clutter only environment. Since the MTI has attenuated the ground clutter, the noise dominates the interference with the exception of a few of the lower frequency cells; therefore, no weighting provides best performance at high frequency cells while degrading performance in the lower cells. This is easily predicted because the rectangular window function has substantial sidelobe coupling in lower cells and obtains the best signal-to noise improvement in noise dominated upper cells. It is also noted that performance degrades as side-lobe levels are lowered because of the reduction in the Signal-to-Noise Ratio caused by the main lobe of the window function.
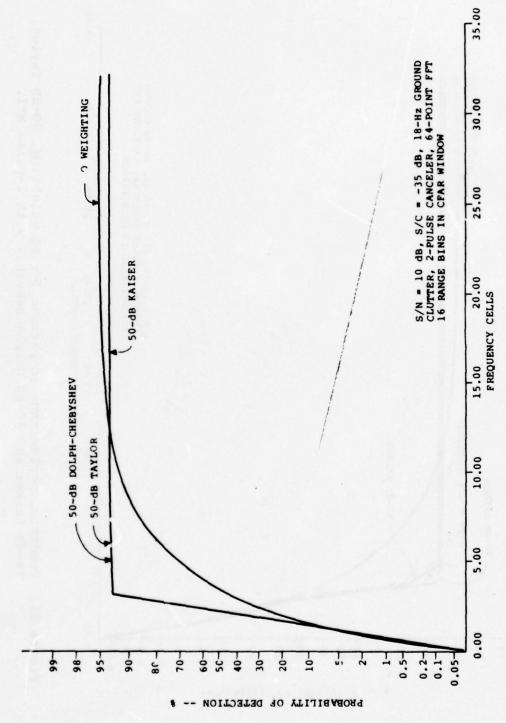
Figures 33 through 36 show results for a ground and weather clutter environment. Several observations can be made. The no weighting system performance is drastically reduced due to sidelobe coupling of weather clutter into other frequency cells. For window functions with similar sidelobe levels the performance is not appreciably different and the differences can be explained by the mainlobe and sidelobe distributions of the window functions. For this particular weather input, the 50-dB window functions provide the best performance which is predictable due to sidelobe levels that are needed to reduce the clutter below the noise. That is, since the input signal-to-noise (S/N) is 10 dB then the output S/N is 28 dB due to FFT improvement. With an input clutter-to-signal (C/S) of 35 dB and an average MTI clutter attenuation of -5.5 dB, the output clutter-to-noise (C/N) is 28 dB plus 29.5 dB which equals 57.5 dB. This implies that the clutter would need to be reduced by 57.5 dB for the noise to be the dominate interference. Hence, sidelobe level needs to be down 57.5 dB. Since 57.5 dB is closer to 50 dB than 70 dB, then the 50-dB window functions should show best performance.

The performance curves shown in Figures 37 through 44 are for a signal processor without an MTI.
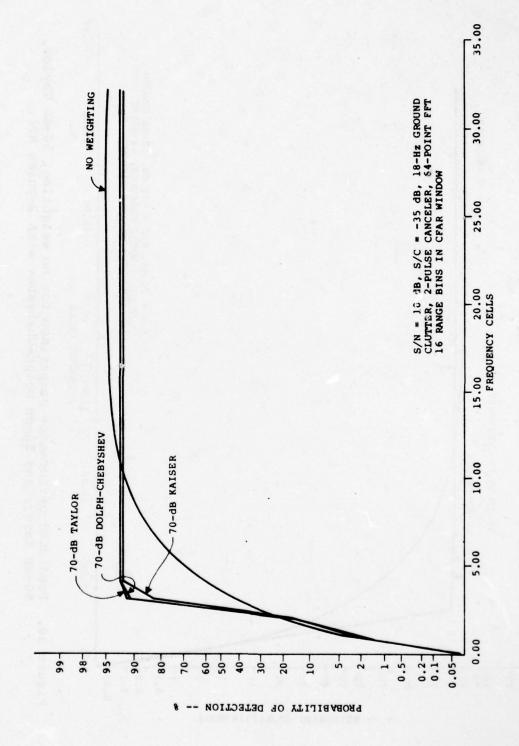
Figures 37 through 40 show results for ground clutter only environment. Since there is no MTI to attenuate the ground clutter, the sidelobe coupling of clutter into all frequency cells tends to reduce performance. In Figure 37 a definite difference in upper frequency cells in performance is noted for the various window functions. The differences are easily explained by the window function sidelobes. The
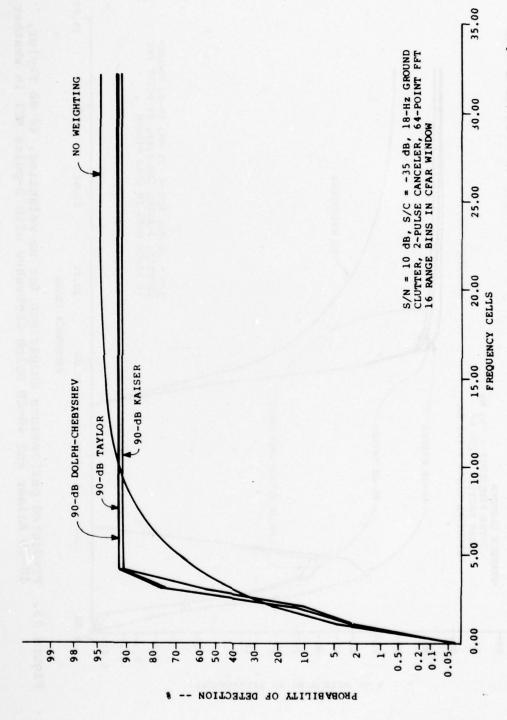
47

Figure 29. Predicted performance comparison for no weighting, 40-dB Taylor, 40-dB Kaiser and 40-dB Dolph-Chebyshev with 2-pulse MTI.

48

Figure 30. Predicted performance comparison for no weighting, 50-dB Taylor, 50-dB Kaiser and 50-dB Dolph-Chebyshev with 2-pulse MTI.

49
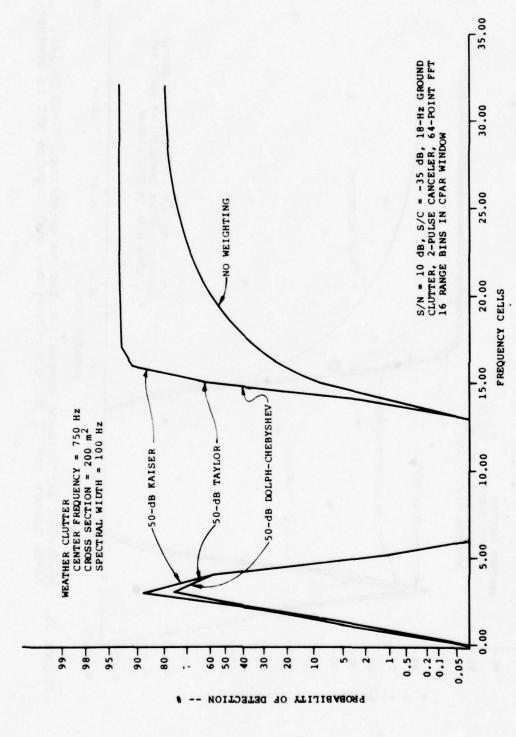
Figure 31. Predicted performance comparison for no weighting, 70-dB Taylor, 70-dB Kaiser and 70-dB Dolph-Chebyshev with 2-pulse MTI.

S/N = 16 dB, S/C = -35 dB, 18-Hz GROUND
CLUTTER, 2-PULSE CANCELER, 64-POINT FFT
16 RANGE BINS IN CFAR WINDOW

Figure 32. Predicted performance comparison for no weighting, 90-dB Taylor, 90-dB Kaiser and 90-dB Dolph-Chebyshev with 2-pulse MTI.

51
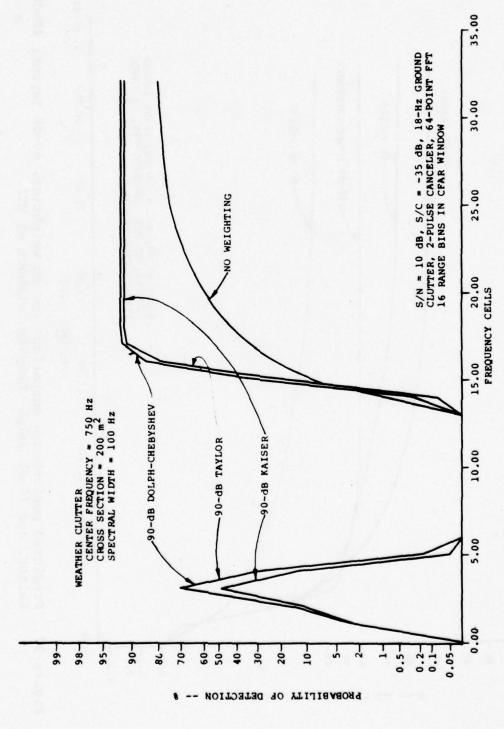
Figure 33. Predicted performance comparison for no weighting, 40-dB Taylor, 40-dB Kaiser and 40-dB Dolph-Chebyshev with 2-pulse MTI in weather.

WEATHER CLUTTER
  CENTER FREQUENCY = 750 Hz
  CROSS SECTION = 200 m²
  SPECTRAL WIDTH = 100 Hz

S/N = 10 dB, S/C = -35 dB, 18-Hz GROUND
CLUTTER, 2-PULSE CANCELER, 64-POINT FFT
16 RANGE BINS IN CFAR WINDOW

52

Figure 34. Predicted performance comparison for no weighting, 50-dB Taylor, 50-dB Kaiser and 50-dB Dolph-Chebyshev with 2-pulse MTI in weather.

53

WEATHER CLUTTER
CENTER FREQUENCY = 750 Hz
CROSS SECTION = 200 m²
SPECTRAL WIDTH = 100 Hz

S/N = 10 dB, S/C = -35 dB, 18-Hz GROUND
CLUTTER, 2-PULSE CANCELER, 64-POINT FFT
16 RANGE BINS IN CFAR WINDOW

Figure 35. Predicted performance comparison for no weighting, 70-dB Taylor,
70-dB Kaiser and 70-dB Dolph-Chebyshev with 2-pulse MTI in weather.

54
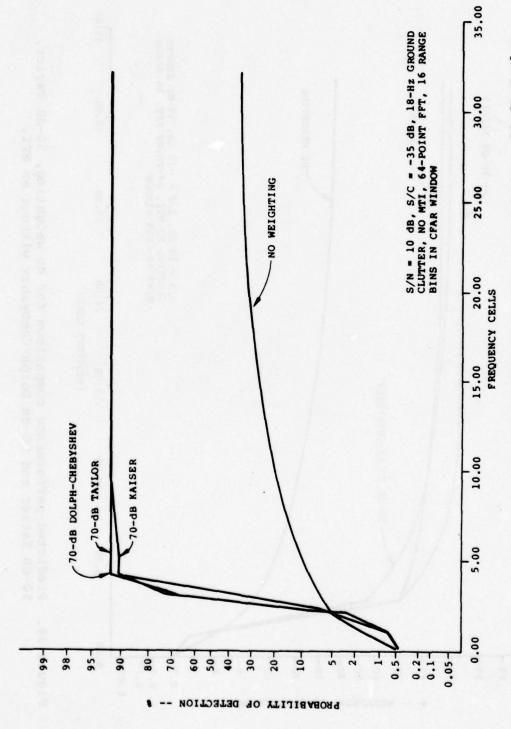
Figure 36. Predicted performance comparison for no weighting, 90-dB Taylor, 90-dB Kaiser and 90-dB Dolph-Chebyshev with 2-pulse MTI in weather.

55

Figure 37. Predicted performance comparison for no weighting, 40-dB Taylor, 40-dB Kaiser, and 40-dB Dolph-Chebyshev without an MTI.

56
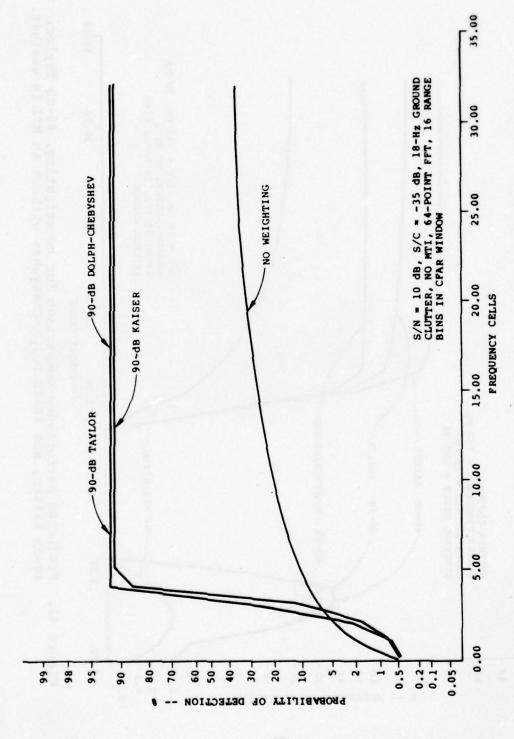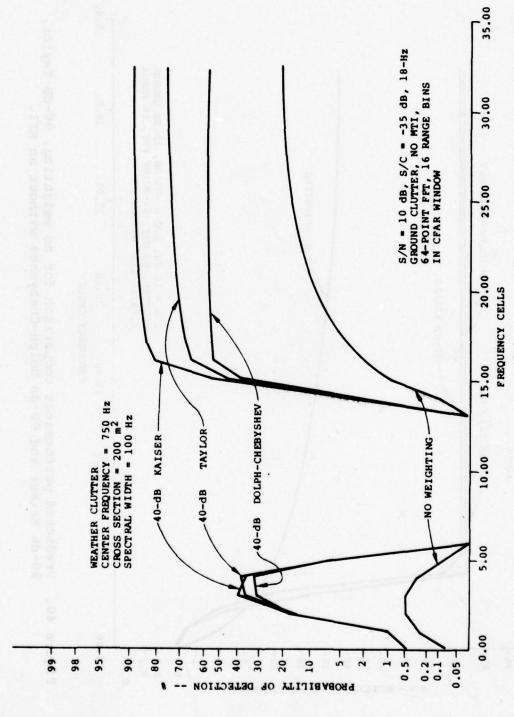
Figure 38. Predicted performance comparison for no weighting, 50-dB Taylor, 50-dB Kaiser and 50-dB Dolph-Chebyshev without an MTI.
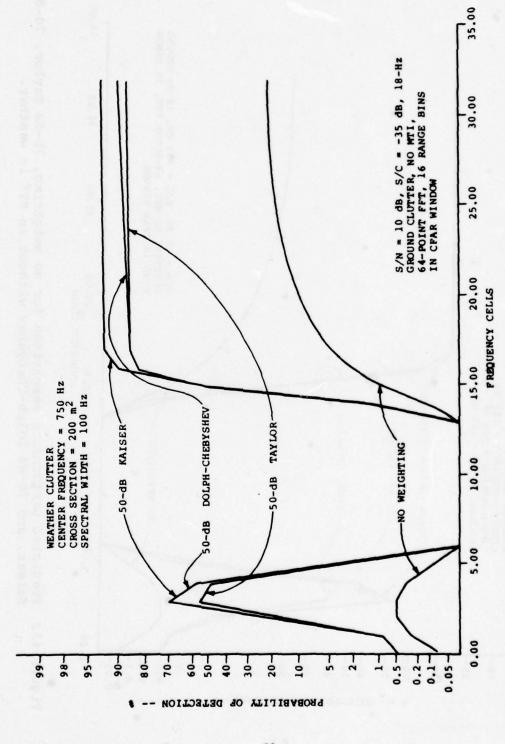
Figure 39.   Predicted performance comparison for no weighting, 70-dB Taylor, 70-dB Kaiser and 70-dB Dolph-Chebyshev.
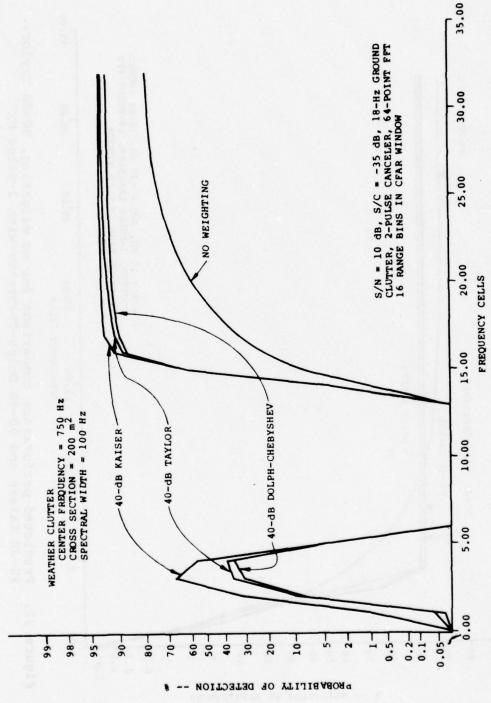
Figure 40. Predicted performance comparison for no weighting, 90-dB Taylor, 90-dB Kaiser and 90-dB Dolph-Chebyshev without an MTI.

59

Figure 41. Predicted performance comparison for no weighting, 40-dB Taylor, 40-dB Kaiser, and 40-dB Dolph-Chebyshev without an MTI in weather.

60

Figure 42. Predicted performance comparison for no weighting, 50-dB Taylor, 50-dB Kaiser, and 50-dB Dolph-Chebyshev without an MTI in weather.

Figure 43. Predicted performance comparison for no weighting, 70-dB Taylor, 70-dB Kaiser, and 70-dB Dolph-Chebyshev without an MTI in weather.

WEATHER CLUTTER
CENTER FREQUENCY = 750 Hz
CROSS SECTION = 200 m^2
SPECTRAL WIDTH = 100 Hz

S/N = 10dB, S/C = -35 dB, 18-Hz
GROUND CLUTTER, NO MTI,
64-POINT FFT, 16 RANGE BINS
IN CFAR WINDOW

90-dB DOLPH-CHEBYSHEV
90-dB TAYLOR
90-dB KAISER
NO WEIGHTING

PROBABILITY OF DETECTION -- %

FREQUENCY CELLS

Figure 44. Predicted performance comparison for no weighting, 90-dB Taylor, 90-dB Kaiser, and 90-dB Dolph-Chebyshev without an MTI in weather.
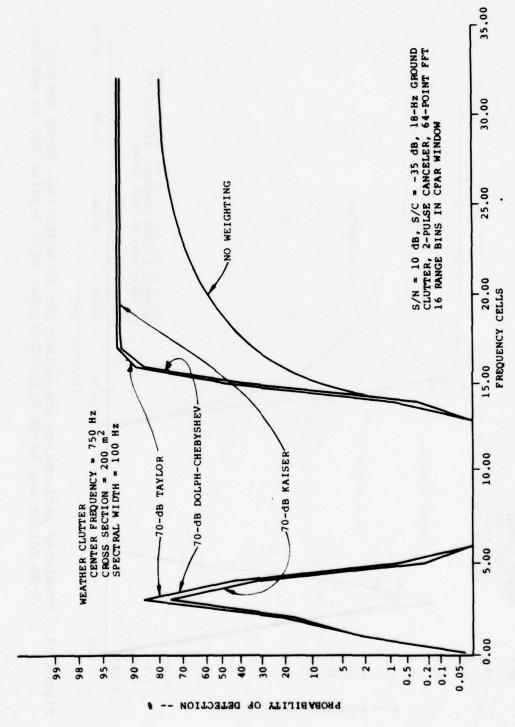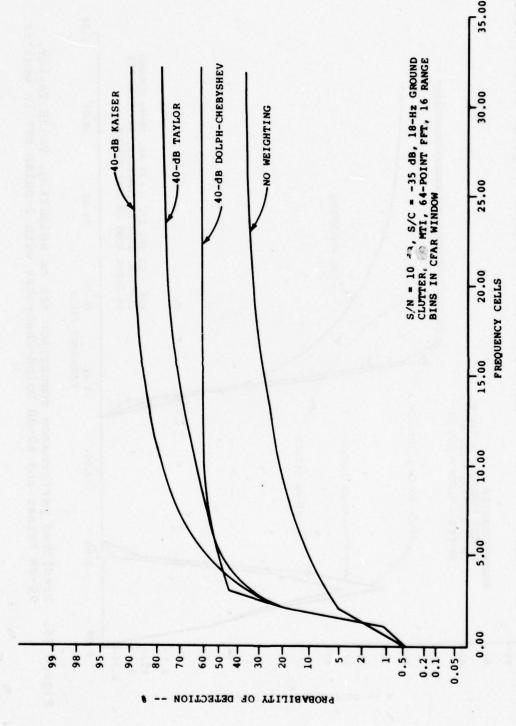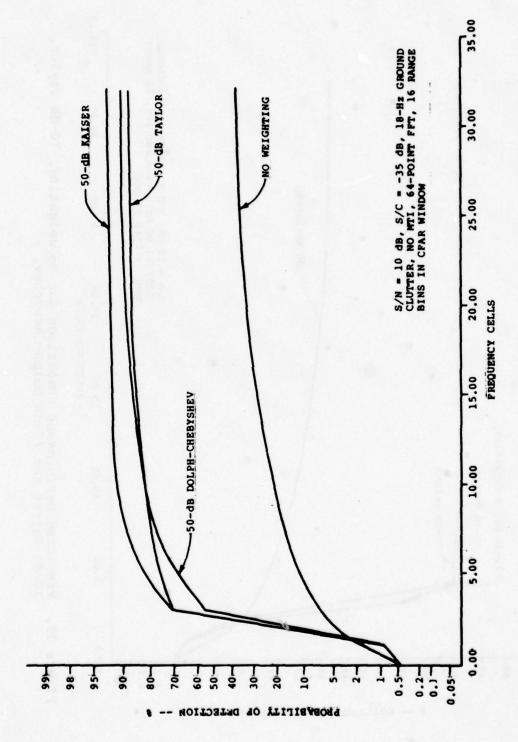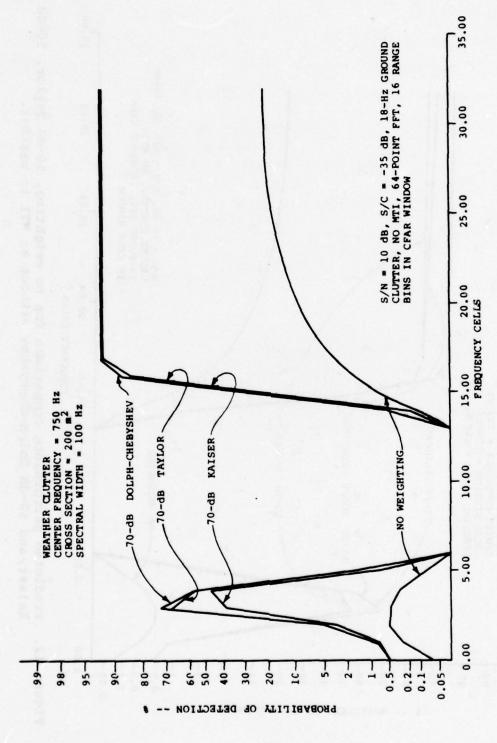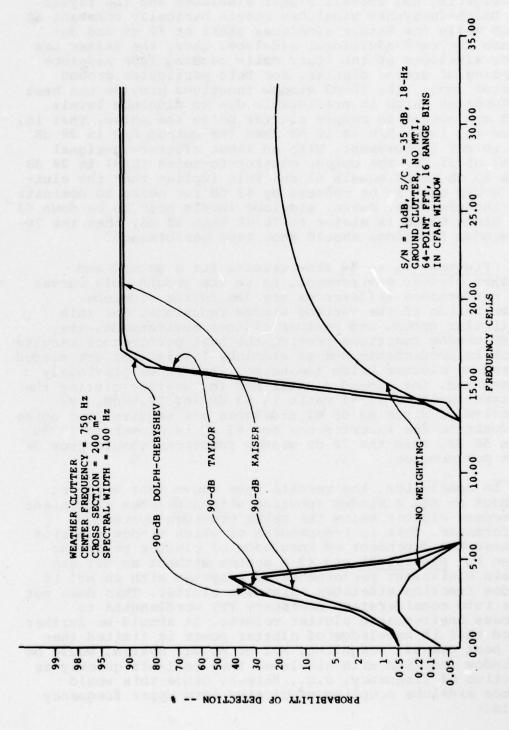
no weighting has overall higher sidelobes and the Taylor
and Dolph-Chebyshev sidelobes remain basically constant at
40 dB while the Kaiser sidelobes start at 40 dB and de-
crease for each additional sidelobe. Thus, the Kaiser has
lower sidelobes at the lower cells causing less sidelobe
coupling of ground clutter. For this particular ground
clutter input, the 70-dB window functions provide the best
performance which is predictable due to sidelobe levels
that are needed to reduce clutter below the noise. That is,
since the input S/N is 10 dB then the output S/N is 28 dB
due to FFT improvement. With an input clutter-to-signal
(C/S) of 35 dB, the output clutter-to-noise (C/N) is 28 dB
plus 35 dB which equals 63 dB. This implies that the clut-
ter would need to be reduced by 63 dB for noise to dominate
the interference. Hence, sidelobe levels need to be down 63
dB. Since 63 dB is closer to 70 dB than 50 dB, then the 70-
dB window functions should show best performance.

Figures 41 to 44 show results for a ground and
weather clutter environment. As in the ground only curves
the performance differences are due to the sidelobe
distribution of the various window functions. For this
particular ground and weather clutter environment, the
70 dB window functions provide the best performance results
which is predictable due to sidelobe levels that are needed
to reduce clutter below the noise. That is as previously
determined, for ground clutter and for weather clutter the
clutter-to-noise (C/N) ratio is 63 dB and 57.5 dB, re-
spectively. Since 63 dB of sidelobes are required for noise
to dominate the interference and 63 dB is closer to 70 dB
than 50 dB, then the 70 dB window functions should provide
best performance.

In conclusion, the results have shown that with or
without an MTI a window function with sidelobes sufficient
to reduce clutter below the noise provides optimum
performance. This is independent of which window function
is used but dependent on knowledge of clutter power. As
shown in Figures 39 and 43 a system without an MTI can
obtain equivalent performance to a system with an MTI if
window function sidelobes eliminate clutter. This does not
take into consideration necessary FFT wordlengths to
process unattenuated clutter returns. It should be further
noted that if knowledge of clutter power is limited then
the best overall weighting, MTI or no MTI system, would be
a window function with sidelobes that roll-off quickly as
function of frequency, e.g., Kaiser, since this would
reduce sidelobe coupling of clutter into upper frequency
cells.

64

6. PROPOSED EXTENSIONS

There are a number of areas that should receive additional studies. Many parameters are involved in specifying the conditions of a computer run, and it is not feasible to create a complete set of performance curves. The following list of additional runs should provide more insight into the performance of the CFAR processor.

1. Vary the signal-to-noise ratio, signal-to-clutter ratio and the weather rate.

2. Vary the center frequency of the weather. The analysis is limited to low center frequencies and to "high" center frequencies.

3. Vary the spectral widths of the ground clutter and the weather clutter.

4. Change the number of FFT points such that the total number of input pulses remain approximately constant as the MTI type is varied. The above runs will not require program modification. A number of items that are of sufficient interest to warrant the effort required for program change are listed below.

5. Add frequency-averaging CFAR by determining a threshold for range-bin j and frequency cell k as

$$D_{jk} = \frac{K_3}{L-1} \sum_{\substack{m=1 \\ m \neq k}}^{L} z_{jm} \tag{31}$$

An alternative is to only exclude the spectral magnitudes of the greatest and then use this threshold for all frequency cells in the jth range bin.

6. Add the capability for non-coherent integration. This appears to be a major change since a closed form of the performance equations are not known when CFAR is used. However, the fixed threshold equation for probability of

65

detection can be obtained from Equation (3-56) of Meyer and Mayer.[9] The fixed threshold probability of false alarm calculations are given by Equation (2-17) of Meyer and Mayer.[9] The program modifications required for CFAR would use the referenced results and the p.d.f. descriptions for the threshold to calculate expected values of the performance results.

7. A major change in the computer program concept is needed to investigate the effectiveness of the Raytheon threshold selection technique as described by Equations (27) and (28). One possibility is to develop subroutines for random selection of values according to the p.d.f. descriptions for the various CFAR/clutter-map thresholds. Monte-Carlo passes through these selections and determining the largest value could then be used to calculate the expected value of the performance statistics.

9. D.P. Meyer, and H.A. Mayer, Radar Target Detection, Academic Press, New York, 1973.

66

REFERENCES

1. Raytheon Company, Automatic Threshold Detector Techniques, Final Report on Contract No. DAAH01-76-C-0363 for US Army Missile Command, ER76-4208, 15 July 1976.

2. Houts, R. C., and Burlage, D. W., "Maximizing the Usable Bandwidth of MTI Signal Processors," Institute of Electrical and Electronics Engineers (IEEE) Transactions on Aerospace and Electronic Systems, Vol. AES-13, No. 1, January 1977, pp. 48-55.

3. Burlage, D. W. and Houts, R. C., Design Techniques for Improved Bandwidth Moving Target Indicator Processors in Surface Radars, US Army Missile Command, Redstone Arsenal, Alabama, Technical Report RE-75-35, 1975.

4. Holt, B.P., and R.C. Houts, "Multiband FIR Digital Filter Design Algorithm for Radar Clutter Suppression," Record of 1978 IEEE Int. Conf. on Acoustics, Speech and Signal Processing, April 1978.

5. Lawrence, N. B. and Moore, J. D., Tradeoff of Hardware and Signal-to-Noise Ratio in Moving Targets Indicators, US Army Missile Research and Development Command, Redstone Arsenal, Alabama, Technical Report T-78-39, 1978.

6. Cook, E. E. and Bernfeld, M., Radar Signals: An Introduction to Theory and Application, Academic Press, New York, 1967.

7. Stanley, W. D. Digital Signal Processing, Prentice-Hall, Virginia, 1975.

8. Polge, et. al., Analog-to-Digital Converter Evaluation by Digital Computer Analysis or Recorded Output, US Army Missile Command, Redstone Arsenal, Alabama, Final Report on Contract No. DAAH01-71-C-1181, 1974.

9. Meyer, D. P. and Mayer, H. A., Radar Target Detection, Academic Press, New York, 1973.

APPENDIX A

MTI OUTPUT NOISE SPECTRAL DENSITY ANALYSIS

The linear system in Figure A-1 where $h(t) = C_0 \delta(t) + C_1 \delta(t-T) + \cdots + C_{N-1} \delta(t-(N-1) \cdot T)$ and $T = 1/f_{in}$ is time-invariant only when f_{out} equals f_{in} and the coefficients $C_0, C_1, \cdots C_{N-1}$ are constants. That is, the system is time-invariant for the moving window inplementation where f_{out} equals f_{in} and is time-varying for the fixed window implementation where f_{out} equals f_{in}/N.

x(t _____ f_in ____ [MTI h(t)] ____ f_out ____ y(t)
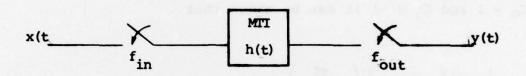
Figure A-1. Linear system

Since the moving window MTI is a time-invariant linear system, the power spectral density at the output has been shown from linear system analysis to be

$$\bar{\Phi}_{yy}(f) = \bar{\Phi}_{xx}(f) \cdot \left| H(f) \right|^2 \qquad (A.1)$$

where $\bar{\Phi}_{xx}(f)$ is the power spectral density of the input and $|H(f)|^2$ is the magnitude squared MTI response. Assuming the input is white Gaussian noise, the input power spectral density is given by

$$\bar{\Phi}_{xx}(f) = \sigma^2 \qquad (A.2)$$

71

Then, the output power spectral density is

$$\overline{\Phi}_{yy}(f) = \sigma^2 |H(f)|^2 . \tag{A.3}$$

Hence, the moving window MTI output noise spectral density is shaped by the MTI response.

For example, if the MTI is a 2-pulse canceler where $C_0 = 1$ and $C_1 = -1$ it can be shown that

$$|H(f)|^2 = 4 \cdot \sin^2 \left(\frac{\pi f}{f_{in}} \right) , \tag{A.4}$$

Substituting (A.2) and (A.4) into (A.1) we have

$$\overline{\Phi}_{yy}(f) = 4\sigma_{\downarrow}^2 \sin^2 \left(\frac{\pi f}{f_{in}} \right) . \tag{A.5}$$

Since the fixed window implementation is a time-varying linear system, the output power spectral density $\overline{\Phi}_{yy}(f)$ cannot be determined by Equation A.1. One technique for determining $\overline{\phi}_{yy}(f)$ is to find the autocorrelation function $\overline{\phi}_{yy}(n\ell)$ which forms a Fourier transform pair with $\overline{\phi}_{yy}(f)$.

For a fixed window MTI, the output is calculated as

$$y(kN) = \sum_{n=0}^{N-1} C_n x (kN - n), \quad k = 1, 2, \ldots K_{FW}, \tag{A.6}$$

where for simplicity T has been dropped from the argument of y( ) and x( ). Then the discrete autocorrelation function $\overline{\phi}_{yy}(\ell)$ is

72

$$\bar{\phi}_{yy}(m) = 0, \ m \neq \ell N, \ \ell = 1,2,\ldots$$

$$\bar{\phi}_{yy}(\ell n) = \overline{y(kN) \cdot y\left(\left[k + \ell\right] \cdot N\right)}^{k}$$

$$= \overline{\sum_{n=0}^{N-1} c_n \ x \ (kN - n) \cdot \sum_{j=0}^{N-1} c_j \ x \left(\left[k + \ell\right] \cdot N - j\right)}$$

$$= \sum_{n=0}^{N-1} \sum_{j=0}^{N-1} c_n c_j \ \overline{x \ (kN - n) \cdot x \left(\left[k + \ell\right] \cdot N - j\right)}.$$

$$= \sum_{n=0}^{N-1} \sum_{j=0}^{N-1} c_n c_j \ \bar{\phi}_{xx} \ (\ell N + n - j) \tag{A.7}$$

Letting $x(t)$ be white Gaussian noise with a discrete autocorrelation function of

$$\bar{\phi}_{xx}(n) = \sigma^2, \ n = 0$$
$$= 0, \ n \neq 0 \tag{A.8}$$

where σ^2 is the noise variance.

Then the term $\overline{x \ (kN - n) \cdot x \ (\left[k + \ell\right] \cdot N - j)}$ in Equation (A.7) is non-zero only for $kN-n = (k + \ell) \ N - j$ or $j = n + \ell N$. Since $0 \leq j \geq N - 1$ then the solution is $\ell = 0$ and $j = n$.

Hence,

$$\bar{\phi}_{yy}(0) = \sum_{n=0}^{N-1} c_n^2 \cdot \bar{\phi}_{xx}(0) \tag{A.9}$$

$$= \sum_{n=0}^{N-1} c_n^2 \cdot \sigma^2$$

73

Therefore, the output discrete autocorrelation function of a fixed window MTI is given by

$$\bar{\phi}_{yy}(\ell N) = \sum_{n=0}^{N-1} C_n^2 \sigma^2 = K\sigma^2, \quad \ell = 0$$

$$= 0 \quad , \ell \neq 0$$

(A.10)

and the output power spectral density is given by

$$\bar{\phi}_{yy}(f) = K\sigma^2$$

(A.11)

Hence, the fixed window MTI output noise spectral density is constant.

For example, if the MTI is a 2-pulse canceler where $C_O = 1$ and $C_1 = -1$, then the power spectral density is,

$$\bar{\phi}_{yy}(f) = \sum_{n=0}^{N-1} C_n^2 \sigma^2 = 2.\sigma^2.$$

(A.12)

74

APPENDIX B

FIXED WINDOW MTI ALIASING

MTIs can be implemented either as a moving window or a fixed window filter. A moving window MTI produces an output for each additional input after N inputs have entered the filter where N is the number of filter coefficients. The fixed window produces one output for each block of N inputs that enters. Whereas the moving window MTI provides more outputs for integration, the use of a fixed window MTI can reduce hardware requirements.[5]

When a fixed window MTI is used with the FFT system, there can be substantial aliasing problems. Figure B-1A shows the frequency domain representations for two targets with one below and the other above fs/3. Figure B-1B shows a representation of the target velocity ambiguity resulting from a fixed window three-pulse canceler. The two-sided clutter spectra shown in Figure B-1C are translated to frequencies (as shown in Figure B-1D and E) where they can interfere with targets. A moving window MTI would result in the FFT frequency range being from 0 Hz to the sampling frequency f_s. The fixed window system effactually reduces the sample rate at the input to the FFT, thus for the three-pulse canceler the range becomes 0 Hz to one-third of the original sampling frequency, i.e., $f_s/3$. Based on this reduction in frequency range and considering the additional clutter interference that is introduced, it is difficult to justify the hardware reduction that could be obtained by the fixed window implementation.

77

A. QUADRATURE SIGNAL INPUT
   FOR TWO TARGETS

TARGET 1

TARGET 2

$\frac{fs}{6}$ $\frac{fs}{3}$ $\frac{fs}{2}$ $\frac{2}{3}fs$ $\frac{5}{6}fs$

B. FIXED WINDOW 3 PC OUTPUT
   FOR TARGET INPUTS

C. CLUTTER SIGNAL INPUT

$\frac{fs}{3}$

D. FIXED WINDOW 3 PC OUTPUT
   FOR CLUTTER INPUT

$\frac{fs}{3}$

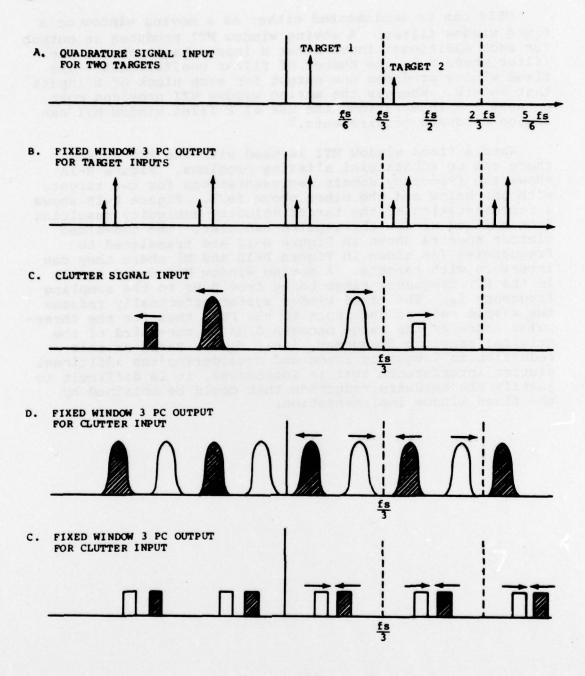C. FIXED WINDOW 3 PC OUTPUT
   FOR CLUTTER INPUT

$\frac{fs}{3}$

Figure B-1. Spectral properties of fixed window 3-pulse
            canceler output with target/clutter inputs.

78

DISTRIBUTION

Defense Documentation Center
Cameron Station
Alexandria, Virginia 22314   12

US Army Materiel Systems Analysis Activity
ATTN: DRXSY-MP
Aberdeen Proving Ground, Maryland 21005   1

Commander
US Army Materiel Development
and Readiness Command
ATTN: DRCCG   1
       DRCRD   1
5001 Eisenhower Avenue
Alexandria, Virginia 22304

Commander
Ballistic Missile Defense Systems Command
ATTN: BMDSC-HR   1
P.O. Box 1500
Huntsville, Alabama 35807

Director
Ballistic Missile Defense
Advanced Technology Center
ATTN: ATC-R   2
P.O. Box 1500
Huntsville, Alabama 35807

Commander
US Army Electronics Research
and Development Command
ATTN: DRSEL, Mr. Fishbien   1
       DRCPM-MALR   1
Fort Monmouth, New Jersey

IIT Research Institute
ATTN: GACIAC   1
10 West 35th Street
Chicago, Illinois 60616

DISTRIBUTION (Concluded)

	No. of Copies
DRCPM-MDE, Mr. Evans	1
-HAE, Mr. Ams	1
-ROL, Mr. Bishop	1
DRSMI-LP, Mr. Voigt	1
DRSMI-T, Dr. Kobler	1
-T, Mr. Fagan	1
-TE, Mr. Lindberg	1
-TE, Mr. Pittman	1
-TEO, Mr. Currie	1
-TEG, Mr. Cash	1
-TER, Mr. Low	1
-TER, Mr. Lawrence	50
-TE, Record Set	1
-TG, Mr. Huff	1
-TD, Dr. McCorkle	1
-TBL	5
-TBD	3
-TI (Reference copy)	1
-TI (Record set)	1

80